NUCLEAR
PHYSICS A

ELSEVIER

Neutrino opacities in nuclear matter

Adam Burrows [a],*, Sanjay Reddy [b], Todd A. Thompson [c]

[a] *Steward Observatory, The University of Arizona, Tucson, AZ 85721, USA*
[b] *Theoretical Division, Los Alamos National Laboratory, Los Alamos, NM 87544, USA*
[c] *Astronomy Department and Theoretical Astrophysics Center, The University of California, Berkeley, CA 94720, USA*

Abstract

Neutrino–matter cross sections and interaction rates are central to the core-collapse supernova phenomenon and, very likely, to the viability of the explosion mechanism itself. In this paper, we describe the major neutrino scattering, absorption, and production processes that together influence the outcome of core collapse and the cooling of protoneutron stars. One focus is on energy redistribution and many-body physics, but our major goal is to provide a useful resource for those interested in supernova neutrino microphysics.
© 2004 Elsevier B.V. All rights reserved.

Keywords: Supernovae; Neutrino interactions; Neutrino spectra; Protoneutron stars; Kinetic theory

1. Introduction

Supernova explosions are one major means by which elements are injected into the interstellar medium and, hence, into subsequent generations of stars. Therefore, supernovae are central to the chemical evolution and progressive enrichment of the universe. Most supernova explosions are the outcome of the dynamical collapse of the core of a massive star as it dies. Collapse creates high temperatures (> 1 MeV) and densities

* Corresponding author.
  E-mail addresses: burrows@zenith.as.arizona.edu (A. Burrows), reddy@lanl.gov (S. Reddy), thomp@astro.berkeley.edu (T.A. Thompson).

$(10^7 \, \mathrm{g\,cm^{-3}} < \rho < 10^{15} \, \mathrm{g\,cm^{-3}})$ and produces ("after the dust settles") either a neutron star or a black hole. Under such extreme thermodynamic conditions, neutrinos are produced in abundance. The mechanism of core-collapse supernovae is thought to depend upon the transfer of energy from the inner core to the outer mantle of the iron core of the massive star. Neutrinos seem to be the mediators of this energy transfer. Therefore, to fully understand core-collapse supernova explosions one must have a firm handle on the physics of neutrino production, absorption, and scattering.

In this paper, we summarize the neutrino–matter cross sections and the neutrino production rates in the core-collapse context. Some of this discussion can already be found in [17]. We do not attempt to explain the hydrodynamics of supernova explosions, but do try to present the relevant neutrino processes that play a role. For the former, the reader is referred to [10,12,15,44,45,57,66].

In Section 2, we present a physical derivation of stimulated absorption and then in Section 3 we summarize the basic neutrino–matter cross sections. In Section 4, we discuss the neutrino–electron scattering kernel, along with a simple treatment of the collision integral. In Section 5, we provide the relativistic formalism for inelastic neutrino–electron and neutrino–nucleon scattering processes and energy redistribution for non-interacting nucleons. This is followed in Section 6 with a discussion of the alternate, more powerful, formalism for determining differential interaction rates and redistribution in the many-body context, namely that of dynamical structure factors. The role of strong and electromagnetic interactions between nucleons and leptons is explored, as well as collective excitations of the medium. Source terms for electron–positron annihilation (Section 7), neutrino–anti-neutrino annihilation (Section 8), and nucleon–nucleon bremsstrahlung (Section 9) cap off our review of the major processes of relevance in core-collapse simulations.

2. Stimulated absorption

The concept of stimulated emission for photons is well understood and studied, but the corresponding concept of stimulated *absorption* for neutrinos is not so well appreciated. This may be because its simple origin in Fermi blocking and the Pauli exclusion principle in the context of *net* emission is not often explained. The *net* emission of a neutrino is simply the difference between the emissivity and the absorption of the medium:

$$\mathcal{J}_{\mathrm{net}} = \eta_\nu - \kappa_a I_\nu, \tag{1}$$

where κ_a is the absorptive opacity and I_ν is the specific intensity. All absorption processes involving fermions will be inhibited by Pauli blocking due to final-state occupancy. Hence, η_ν in Eq. (1) includes a blocking term, $(1 - \mathcal{F}_\nu)$ [7]. $\mathcal{F}_\nu$ is the invariant distribution function for the neutrino, whether or not it is in chemical equilibrium.

We can derive stimulated absorption using Fermi's Golden rule. For example, the net collision term for the process, $\nu_e n \leftrightarrow e^- p$, is:

$$\mathcal{C}_{\nu_e n \leftrightarrow e^- p} = \int \frac{d^3 \vec{p}_{\nu_e}}{(2\pi)^3} \int \frac{d^3 \vec{p}_n}{(2\pi)^3} \int \frac{d^3 \vec{p}_p}{(2\pi)^3} \int \frac{d^3 \vec{p}_e}{(2\pi)^3} \left(\sum_s |\mathcal{M}|^2 \right)$$
$$\times \, \Xi(\nu_e n \leftrightarrow e^- p)(2\pi)^4 \delta^4(\mathbf{p}_{\nu_e} + \mathbf{p}_n - \mathbf{p}_p - \mathbf{p}_e), \tag{2}$$

where **p** is a four-vector and

$$\Xi(\nu_e n \leftrightarrow e^- p) = \mathcal{F}_{\nu_e}\mathcal{F}_n(1 - \mathcal{F}_e)(1 - \mathcal{F}_p) - \mathcal{F}_e\mathcal{F}_p(1 - \mathcal{F}_n)(1 - \mathcal{F}_{\nu_e}). \tag{3}$$

The final-state blocking terms in Eq. (3) are manifest, in particular that for the ν_e neutrino. Algebraic manipulations convert $\Xi(\nu_e n \leftrightarrow e^- p)$ in Eq. (3) into:

$$\begin{aligned}
\Xi(\nu_e n \leftrightarrow e^- p) &= \mathcal{F}_n(1 - \mathcal{F}_e)(1 - \mathcal{F}_p)\left[\frac{\mathcal{F}_{\nu_e}^{\text{eq}}}{1 - \mathcal{F}_{\nu_e}^{\text{eq}}}(1 - \mathcal{F}_{\nu_e}) - \mathcal{F}_{\nu_e}\right] \\
&= \frac{\mathcal{F}_n(1 - \mathcal{F}_e)(1 - \mathcal{F}_p)}{1 - \mathcal{F}_{\nu_e}^{\text{eq}}}[\mathcal{F}_{\nu_e}^{\text{eq}} - \mathcal{F}_{\nu_e}],
\end{aligned} \tag{4}$$

where

$$\mathcal{F}_{\nu_e}^{\text{eq}} = \left[e^{(\varepsilon_{\nu_e} - (\mu_e - \hat{\mu}))\beta} + 1\right]^{-1} \tag{5}$$

is an equilibrium distribution function for the ν_e neutrino and it has been assumed that only the electron, proton, and neutron are in thermal equilibrium. $\hat{\mu}$ is the difference between the neutron and the proton chemical potentials. Note that in $\mathcal{F}_{\nu_e}^{\text{eq}}$ there is no explicit reference to a neutrino chemical potential, though of course in beta equilibrium it is equal to $\mu_e - \hat{\mu}$. There is no need to construct or refer to a neutrino chemical potential in neutrino transfer.

We see that Eq. (4) naturally leads to:

$$\mathcal{J}_{\text{net}} = \frac{\kappa_a}{1 - \mathcal{F}_\nu^{\text{eq}}}(B_\nu - I_\nu) = \kappa_a^*(B_\nu - I_\nu). \tag{6}$$

Of course, B_ν is the black body function for neutrinos. This expression emphasizes the fact that $\mathcal{C}_{\nu_e n \leftrightarrow e^- p}$ and $\mathcal{J}_{\text{net}}$ are the same entity. If neutrinos were bosons, we would have found a $(1 + \mathcal{F}_\nu^{\text{eq}})$ in the denominator, but the form of Eq. (6) in which I_ν is manifestly driven to B_ν, the equilibrium intensity, would have been retained. From Eqs. (4) and (6), we see that the stimulated absorption correction to κ_a is $1/(1 - \mathcal{F}_\nu^{\text{eq}})$. By writing the collision term in the form of Eq. (6), with κ_a corrected for stimulated absorption, we have a net source term that clearly drives I_ν to equilibrium. The timescale is $1/c\kappa_a^*$. Though the derivation of the stimulated absorption correction we have provided here is for the $\nu_e n \leftrightarrow e^- p$ process, this correction is quite general and applies to all neutrino absorption opacities.

Kirchhoff's Law, expressing detailed balance, is:

$$\kappa_a = \eta_\nu/B_\nu \quad \text{or} \quad \kappa_a^* = \eta_\nu'/B_\nu, \tag{7}$$

where η_ν' is not corrected for final-state neutrino blocking. Furthermore, the net emissivity can be written as the sum of its *spontaneous* and *induced* components:

$$\eta_\nu = \kappa_a\left[\frac{B_\nu}{1 \pm \mathcal{F}_\nu^{\text{eq}}} + \left(1 - \frac{1}{1 \pm \mathcal{F}_\nu^{\text{eq}}}\right)I_\nu\right], \tag{8}$$

where $+$ or $-$ is used for bosons or fermions, respectively. Eq. (7) can be used to convert the absorption cross sections described in Section 3 into source terms.

3. Neutrino cross sections

Neutrino–matter cross sections, both for scattering and for absorption, play the central role in neutrino transport. The major processes are the super-allowed charged-current absorptions of ν_e and $\bar{\nu}_e$ neutrinos on free nucleons, neutral–current scattering off of free nucleons, alpha particles, and nuclei [21], neutrino–electron/positron scattering, neutrino–nucleus absorption, neutrino–neutrino scattering, neutrino–anti-neutrino absorption, and the inverses of various neutrino production processes such as nucleon–nucleon bremsstrahlung and the modified URCA process ($\nu_e + n + n \rightarrow e^- + p + n$). Compared with photon–matter interactions, neutrino–matter interactions are relatively simple functions of incident neutrino energy. Resonances play little role and continuum processes dominate. Nice early summaries of the various neutrino cross sections of relevance in supernova theory are given in [67] and in [7]. In particular, Bruenn [7] discusses in detail neutrino–electron scattering and neutrino–anti-neutrino processes using the full energy redistribution formalism. He also provides a practical approximation to the neutrino–nucleus absorption cross section [1,26], though better physics soon promises to improve the treatment of these cross sections substantially [41,52]. For a neutrino energy of ~ 10 MeV the ratio of the charged-current cross section to the ν_e–electron scattering cross section is ~ 100. However, neutrino–electron scattering does play a role, along with neutrino–nucleon scattering and nucleon–nucleon bremsstrahlung, in the energy equilibration of emergent ν_μ neutrinos [65].

Below, we list and discuss many of the absorption and elastic scattering cross sections one needs in detailed supernova calculations. In Sections 4, 5, and 6, we provide some straightforward formulae that can be used to properly handle inelastic scattering. The set of these processes comprises the essential microphysical package for the simulation of neutrino atmospheres and core-collapse supernovae.

3.1. $\nu_e + n \rightarrow e^- + p$

The cross section per baryon for ν_e neutrino absorption on free neutrons is larger than that for any other process. Given the large abundance of free neutrons in protoneutron star atmospheres, this process is central to ν_e neutrino transport. A convenient reference neutrino cross section is σ_o, given by

$$\sigma_o = \frac{4G_F^2 \cos^2(\theta_C)(m_e c^2)^2}{\pi(\hbar c)^4} \simeq 1.705 \times 10^{-44} \text{ cm}^2, \qquad (9)$$

where G_F is the Fermi weak coupling constant ($\simeq 1.436 \times 10^{-49}$ erg cm^{-3}) from muon decay and θ_C is the Cabibbo angle. The total ν_e–n absorption cross section is then given by

$$\sigma_{\nu_e n}^a = \sigma_o \left(\frac{1 + 3g_A^2}{4}\right)\left(\frac{\varepsilon_{\nu_e} + \Delta_{np}}{m_e c^2}\right)^2 \left[1 - \left(\frac{m_e c^2}{\varepsilon_{\nu_e} + \Delta_{np}}\right)^2\right]^{1/2} W_M, \qquad (10)$$

where g_A is the axial–vector coupling constant (~ -1.23), $\Delta_{np} = m_n c^2 - m_p c^2 = 1.293332$ MeV, and for a collision in which the electron gets all of the kinetic energy

$\epsilon_{e^-} = \varepsilon_{\nu_e} + \Delta_{np}$. W_M is the correction for weak magnetism and recoil [68, Section 5] and is approximately equal to $(1 + 1.1\varepsilon_{\nu_e}/m_n c^2)$. At $\varepsilon_{\nu_e} = 20$ MeV, this correction is only $\sim 2.5\%$. We include it here for symmetry's sake, since the corresponding correction $(W_{\bar{M}})$ for $\bar{\nu}_e$ neutrino absorption on protons is $(1 - 7.1\varepsilon_{\bar{\nu}_e}/m_n c^2)$, which at 20 MeV is a large -15%. To calculate κ_a^*, $\sigma_{\nu_e n}^a$ must be multiplied by the stimulated absorption correction, $1/(1 - \mathcal{F}_{\nu_e}^{\text{eq}})$, and final-state blocking by the electrons and the protons à la Eq. (4) must be included.

3.2. $\bar{\nu}_e + p \rightarrow e^+ + n$

The total $\bar{\nu}_e$–p absorption cross section is given by

$$\sigma_{\bar{\nu}_e p}^a = \sigma_o \left(\frac{1 + 3g_A^2}{4}\right) \left(\frac{\epsilon_{\bar{\nu}_e} - \Delta_{np}}{m_e c^2}\right)^2 \left[1 - \left(\frac{m_e c^2}{\epsilon_{\bar{\nu}_e} - \Delta_{np}}\right)^2\right]^{1/2} W_{\bar{M}}, \tag{11}$$

where $\epsilon_{e^+} = \epsilon_{\bar{\nu}_e} - \Delta_{np}$ and $W_{\bar{M}}$ is the weak magnetism/recoil correction given in Section 3.1. Note that $W_{\bar{M}}$ is as large as many other corrections and should not be ignored. To calculate κ_a^*, $\sigma_{\bar{\nu}_e p}^a$ must also be corrected for stimulated absorption and final-state blocking. However, the sign of $\mu_e - \hat{\mu}$ in the stimulated absorption correction for $\bar{\nu}_e$ neutrinos is flipped, as is the sign of μ_e in the positron blocking term. Hence, as a consequence of the severe electron lepton asymmetry in core-collapse supernovae, both coefficients are very close to one. Note that the $\bar{\nu}_e + p \rightarrow e^+ + n$ process dominates the supernova neutrino signal in proton-rich underground neutrino telescopes on Earth, such as Super-Kamiokande, SNO, and LVD, a fact that emphasizes the interesting complementarities between emission at the supernova and detection in Čerenkov and scintillation facilities.

3.3. $\nu_e A \leftrightarrow A' e^-$

From Bruenn [7] the total ν_e–A absorption cross section, is approximated by

$$\sigma_A^a = \frac{\sigma_o}{14} g_A^2 N_p(Z) N_n(N) \left(\frac{\varepsilon_\nu + Q'}{m_e c^2}\right)^2 \left[1 - \left(\frac{m_e c^2}{\varepsilon_\nu + Q'}\right)^2\right]^{1/2} W_{\text{block}}, \tag{12}$$

where $W_{\text{block}} = (1 - f_{e^-}) e^{(\mu_n - \mu_p - Q')\beta}$, $Q' = M_{A'} - M_A + \Delta \sim \mu_n - \mu_p + \Delta$, Δ is the energy of the neutron $1f_{5/2}$ state above the ground state and is taken to be 3 MeV [25], and the quantities $N_p(Z)$ and $N_n(N)$ are approximated by: $N_p(Z) = 0$, $Z - 20$, and 8 for $Z < 20$, $20 < Z < 28$, and $Z > 28$, respectively, and $N_n(N) = 6$, $40 - N$, and 0 for $N < 34$, $43 < N < 40$, and $N > 40$, respectively. The opacity, corrected for stimulated absorption, is then

$$\kappa_a^* = X_H \rho N_A \sigma_A^a \left(1 - \mathcal{F}_{\nu_e}^{\text{eq}}\right)^{-1}. \tag{13}$$

Since $N_n(N) = 0$ for $N > 40$, this absorption and emission process plays a role only during the very early phase of collapse. Typically, at densities near $\rho \sim 10^{12}$ g cm^{-3}, $\kappa_a^* \rightarrow 0$. Eq. (12) is only approximate and better estimates of the ν_e–A absorption cross section are in the offing [41,52].

3.4. $\nu_i + p \rightarrow \nu_i + p$

The total ν_i–p elastic scattering cross section for all neutrino species is:

$$\sigma_p = \frac{\sigma_o}{4}\left(\frac{\varepsilon_\nu}{m_e c^2}\right)^2 \left(4\sin^4\theta_W - 2\sin^2\theta_W + \frac{(1+3g_A^2)}{4}\right), \tag{14}$$

where θ_W is the Weinberg angle and $\sin^2\theta_W \simeq 0.23$. In terms of $C_V' = 1/2 + 2\sin^2\theta_W$ and $C_A' = 1/2$ (note primes), Eq. (14) becomes [62]:

$$\sigma_p = \frac{\sigma_o}{4}\left(\frac{\varepsilon_\nu}{m_e c^2}\right)^2 \left[(C_V' - 1)^2 + 3g_A^2(C_A' - 1)^2\right]. \tag{15}$$

The differential cross section is:

$$\frac{d\sigma_p}{d\Omega} = \frac{\sigma_p}{4\pi}(1 + \delta_p \mu), \tag{16}$$

where

$$\delta_p = \frac{(C_V' - 1)^2 - g_A^2(C_A' - 1)^2}{(C_V' - 1)^2 + 3g_A^2(C_A' - 1)^2}. \tag{17}$$

Note that δ_p, and δ_n below, are negative ($\delta_p \sim -0.2$ and $\delta_n \sim -0.1$) and, hence, that these processes are backward-peaked.

The transport (or momentum-transfer) cross section is simply

$$\sigma_p^{\mathrm{tr}} = \frac{\sigma_o}{6}\left(\frac{\varepsilon_\nu}{m_e c^2}\right)^2 \left[(C_V' - 1)^2 + 5g_A^2(C_A' - 1)^2\right], \tag{18}$$

where

$$\sigma_i^{\mathrm{tr}} = \int \frac{d\sigma_i}{d\Omega}(1 - \mu)\,d\Omega = \sigma_i\left(1 - \frac{1}{3}\delta_i\right). \tag{19}$$

3.5. $\nu_i + n \rightarrow \nu_i + n$

The total ν_i–n elastic scattering cross section is:

$$\sigma_n = \frac{\sigma_o}{4}\left(\frac{\varepsilon_\nu}{m_e c^2}\right)^2 \left(\frac{1 + 3g_A^2}{4}\right). \tag{20}$$

The corresponding differential cross section is:

$$\frac{d\sigma_n}{d\Omega} = \frac{\sigma_n}{4\pi}(1 + \delta_n \mu), \tag{21}$$

where

$$\delta_n = \frac{1 - g_A^2}{1 + 3g_A^2}. \tag{22}$$

The transport cross section is

$$\sigma_n^{\mathrm{tr}} = \frac{\sigma_o}{4}\left(\frac{\varepsilon_\nu}{m_e c^2}\right)^2 \left(\frac{1 + 5g_A^2}{6}\right). \tag{23}$$

The fact that δ_p and δ_n are negative and, as a consequence, that σ_i^{tr} is greater than σ_i increases the neutrino–matter energy coupling rate for a given neutrino flux in the semi-transparent region.

Horowitz [34] derived expressions that include a weak magnetism/recoil correction analogous to those previously discussed for the charged-current absorption rates $\nu_e n \leftrightarrow pe^-$ and $\bar{\nu}_e n \leftrightarrow ne^+$. We take the following form for the weak magnetism/recoil correction, a fit to the actual correction factor for the transport cross sections:

$$\sigma_{n,p}^{\text{tr}} \rightarrow \sigma_{n,p}^{\text{tr}}(1 + C_{W_M}\varepsilon_\nu/m_{n,p}), \tag{24}$$

where for neutrino–neutron scattering $C_{W_M} \simeq -0.766$, for neutrino–proton scattering $C_{W_M} \simeq -1.524$, for anti-neutrino–neutron scattering $C_{W_M} \simeq -7.3656$, and for anti-neutrino–proton scattering $C_{W_M} \simeq -6.874$.

In fact, neutrino–nucleon scattering is slightly inelastic and when this is germane, as with ν_μ and ν_τ neutrinos, the more general formalism of Sections 4–6 is necessary.

3.6. $\nu_i + A \rightarrow \nu_i + A$

In the post-bounce phase, nuclei exist in the unshocked region exterior to the shock. At the high entropies in shocked protoneutron star atmospheres there are very few nuclei. There are alpha particles, but their fractional abundances are generally low, growing to interesting levels due to reassociation of free nucleons just interior to the shock only at late times. However, nuclei predominate on infall and neutrino–nucleus scattering [21] is the most important process during the lepton trapping phase.

The differential ν_i–A neutral–current scattering cross section may be expressed as:

$$\frac{d\sigma_A}{d\Omega} = \frac{\sigma_o}{64\pi}\left(\frac{\varepsilon_\nu}{m_e c^2}\right)^2 A^2 \{\mathcal{W}\mathcal{C}_{\text{FF}} + \mathcal{C}_{\text{LOS}}\}^2 \langle \mathcal{S}_{\text{ion}}\rangle (1 + \mu), \tag{25}$$

where

$$\mathcal{W} = 1 - \frac{2Z}{A}\left(1 - 2\sin^2\theta_W\right), \tag{26}$$

Z is the atomic number, A is the atomic weight, and $\langle\mathcal{S}_{\text{ion}}\rangle$ is the ion–ion correlation function, determined mostly by the Coulomb interaction between the nuclei during infall. $\langle\mathcal{S}_{\text{ion}}\rangle$, in Eq. (25) was investigated by Horowitz [33] who approximated it with the expansion

$$\langle\mathcal{S}_{\text{ion}}(\epsilon)\rangle = \left[1 + \exp\left(-\sum_{i=0}^{6}\beta_i(\Gamma)\epsilon^i\right)\right]^{-1}, \tag{27}$$

where

$$\Gamma = \frac{(Ze)^2}{a}\frac{1}{kT}, \qquad \epsilon_i = \frac{\varepsilon_{\nu_i}}{\hbar ca}, \qquad a = \left(\frac{3}{4\pi n_{\text{ion}}}\right)^{1/3}, \tag{28}$$

a is the interparticle spacing, n_{ion} is the number density of ions, Γ is the ratio of the Coulomb potential between ions to the thermal energy in the medium, and β_i are specified functions of Γ for each neutrino species.

Leinson et al. [43] have investigated the electron polarization correction, $\mathcal{C}_{\text{LOS}}$, and find that

$$\mathcal{C}_{\text{LOS}} = \frac{Z}{A}\left(\frac{1 + 4\sin^2\theta_W}{1 + (kr_{\text{D}})^2}\right), \tag{29}$$

where the Debye radius is

$$r_{\text{D}} = \sqrt{\frac{\pi\hbar^2 c}{4\alpha p_{\text{F}} E_{\text{F}}}}, \tag{30}$$

$k^2 = |\mathbf{p} - \mathbf{p}'|^2 = 2(\varepsilon_\nu/c)^2(1 - \mu)$, p_{F} and E_{F} are the electron Fermi momentum and energy, and α is the fine-structure constant ($\simeq 137^{-1}$). Note that $r_{\text{D}} \sim 10\hbar/p_{\text{F}}$ in the ultra-relativistic limit ($p_{\text{F}} \gg m_e c$). The $\mathcal{C}_{\text{LOS}}$ term is important only for low neutrino energies, generally below ~ 5 MeV.

Following [67] and [11], the form factor term, $\mathcal{C}_{\text{FF}}$, in Eq. (25) can be approximated by:

$$\mathcal{C}_{\text{FF}} = e^{-y(1-\mu)/2}, \tag{31}$$

where

$$y = \frac{2}{3}\varepsilon_\nu^2\langle r^2\rangle/(\hbar c)^2 \simeq \left(\frac{\varepsilon_\nu}{56\text{ MeV}}\right)^2\left(\frac{A}{100}\right)^{2/3},$$

and $\langle r^2\rangle^{1/2}$ is the rms radius of the nucleus. $\mathcal{C}_{\text{FF}}$ differs from 1 for large A and ε_ν, when the de Broglie wavelength of the neutrino is smaller than the nuclear radius.

When $\langle \mathcal{S}_{\text{ion}}\rangle = \mathcal{C}_{\text{FF}} = \mathcal{C}_{\text{LOS}} + 1 = 1$, we have simple coherent Freedman scattering. The physics of the polarization, ion–ion correlation, and form factor corrections to coherent scattering is interesting in its own right, but has little effect on supernovae [8]. The total and transport scattering cross sections for ν_i–α scattering ($Z = 2$; $A = 4$) are simply

$$\sigma_\alpha = \frac{3}{2}\sigma_\alpha^{\text{tr}} = 4\sigma_o\left(\frac{\varepsilon_\nu}{m_e c^2}\right)^2\sin^4\theta_W. \tag{32}$$

4. The neutrino scattering kernel and a simplified approach to inelastic scattering

Many authors have studied inelastic neutrino–electron scattering as an important energy redistribution process which helps to thermalize neutrinos and increase their energetic coupling to matter in supernova explosions [7,48–50]. Comparatively little attention has been paid to inelastic neutrino–nucleon scattering. Thompson et al. [65] and Raffelt [55] showed that, at least for ν_μ and ν_τ neutrinos, this process cannot be ignored. Here, we review the Legendre expansion formalism for approximating the angular dependence of the scattering kernel, detail our own implementation of scattering terms in the Boltzmann equation, and include a discussion of neutrino–nucleon energy redistribution. In Section 5, we present an alternate approach involving dynamical structure factors that is more easily generalized to include many-body effects (Section 6).

The general collision integral (RHS of the Boltzmann equation) for inelastic scattering may be written as

$$\mathcal{L}_\nu^{\text{scatt}}[f_\nu] = (1 - f_\nu) \int \frac{d^3 p_\nu'}{c(2\pi\hbar c)^3} f_\nu' R^{\text{in}}(\varepsilon_\nu, \varepsilon_\nu', \cos\theta)$$

$$- f_\nu \int \frac{d^3 p_\nu'}{c(2\pi\hbar c)^3} (1 - f_\nu') R^{\text{out}}(\varepsilon_\nu, \varepsilon_\nu', \cos\theta) \tag{33}$$

$$= \tilde{\eta}_\nu^{\text{scatt}} - \tilde{\chi}_\nu^{\text{scatt}} f_\nu, \tag{34}$$

where $\cos\theta$ is the cosine of the scattering angle, ε_ν is the incident neutrino energy, and ε_ν' is the scattered neutrino energy. Although we suppress it here, the incident and scattered neutrino phase space distribution functions (f_ν and f_ν', respectively) have the following dependencies: $f_\nu = f_\nu(r, t, \mu, \varepsilon_\nu)$ and $f_\nu' = f_\nu'(r, t, \mu', \varepsilon_\nu')$. μ and μ' are the cosines of the angular coordinate of the zenith angle in spherical symmetry and are related to $\cos\theta$ through

$$\cos\theta = \mu\mu' + \left[\left(1 - \mu^2\right)\left(1 - \mu'^2\right)\right]^{1/2} \cos(\phi - \phi'). \tag{35}$$

The only difference between f_ν and $\mathcal{F}_\nu$ in Section 2 is that here f_ν has explicit μ and ε_ν dependencies. R^{in} is the scattering kernel for scattering into the bin (ε_ν, μ) from any bin (ε_ν', μ') and R^{out} is the scattering kernel for scattering out of the bin (ε_ν, μ) to any bin (ε_ν', μ'). The kernels are Green's functions that connect points in energy and momentum space. One may also write $R(\varepsilon_\nu, \varepsilon_\nu', \cos\theta)$ as $R(q, \omega)$, where $\omega(= \varepsilon_\nu - \varepsilon_\nu')$ is the energy transfer and $q(= [\varepsilon_\nu^2 + \varepsilon_\nu'^2 - 2\varepsilon_\nu \varepsilon_\nu' \cos\theta]^{1/2})$ is the momentum transfer, so that the kernel explicitly reflects these dependencies (Section 5).

An important simplification comes from detailed balance, a consequence of the fact that these scattering rates must drive the distribution to equilibrium. One obtains: $R^{\text{in}} = e^{-\beta\omega} R^{\text{out}}$, where $\beta = 1/T$. Therefore, we need deal only with R^{out}. The scattering kernels for inelastic neutrino–nucleon and neutrino–electron scattering depend in a complicated fashion on scattering angle. For this reason, one generally approximates the angular dependence of the scattering kernel with a truncated Legendre series [7]. We take

$$R^{\text{out}}(\varepsilon_\nu, \varepsilon_\nu', \cos\theta) = \sum_{l=0}^{\infty} \frac{2l + 1}{2} \Phi(\varepsilon_\nu, \varepsilon_\nu', \cos\theta) P_l(\cos\theta), \tag{36}$$

where

$$\Phi_l(\varepsilon_\nu, \varepsilon_\nu') = \int_{-1}^{+1} d(\cos\theta) \, R^{\text{out}}(\varepsilon_\nu, \varepsilon_\nu', \cos\theta) P_l(\cos\theta). \tag{37}$$

Fig. 1 shows $R^{\text{out}}(\varepsilon_\nu, \varepsilon_\nu', \cos\theta)$ for ν–electron scattering as a function of $\cos\theta$ for various values of ε_ν' at $\varepsilon_\nu = 20$ MeV and a representative thermodynamic point. In practice, one expands only to first order so that

$$R^{\text{out}}(\varepsilon_\nu, \varepsilon_\nu', \cos\theta) \sim \frac{1}{2}\Phi_0(\varepsilon_\nu, \varepsilon_\nu') + \frac{3}{2}\Phi_1(\varepsilon_\nu, \varepsilon_\nu') \cos\theta. \tag{38}$$

Fig. 2 depicts the various Legendre contributions for the same point. Fig. 3 provides the corresponding final-state energy distribution function for various values of ε_ν, using only the $l = 0$ term. Figs. 4 and 5 are similar to Figs. 1 and 3, but are for inelastic ν–nucleon scattering at a representative thermodynamic point.
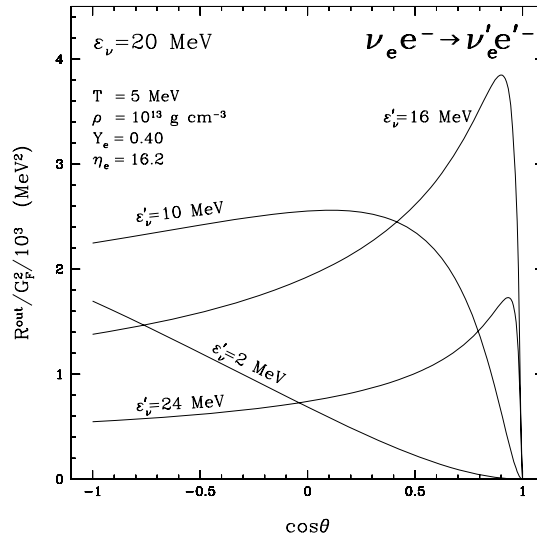
Fig. 1. The scattering kernel $R^{\text{out}}(\varepsilon_\nu, \varepsilon'_\nu, \cos\theta)$ for ν_e–electron scattering as a function of $\cos\theta$ for $\varepsilon_\nu = 20$ MeV and $\varepsilon'_\nu = 2$, 10, 16, and 24 MeV, at a representative thermodynamic point ($T = 5$ MeV, $\rho = 10^{13}$ g cm^{-3}, $Y_e = 0.4$).
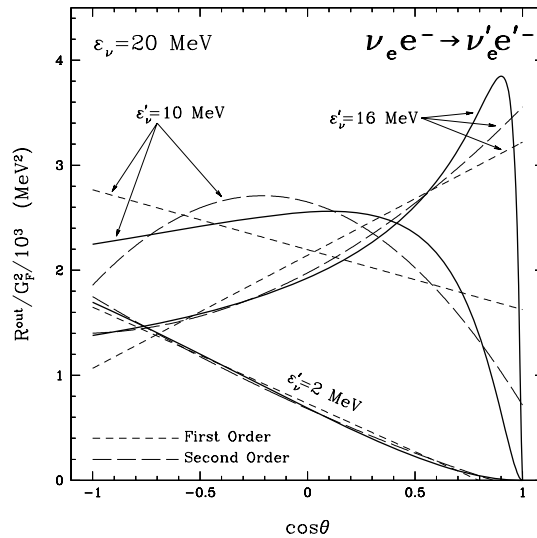

Fig. 2. For the same thermodynamic point as used for Fig. 1, the scattering kernel (R^{out}, thick solid lines) for ν_e–electron scattering as a function of $\cos\theta$, for $\varepsilon_\nu = 20$ MeV and $\varepsilon'_\nu = 2$, 10, and 16 MeV. Short dashed lines show the first-order Legendre series expansion approximation to R^{out}, which is linear in $\cos\theta$; $R^{\text{out}} \sim (1/2)\Phi_0 + (3/2)\Phi_1 \cos\theta$. The long dashed line shows the improvement in going to second order in $\cos\theta$ by taking $R^{\text{out}} \sim (1/2)\Phi_0 + (3/2)\Phi_1 \cos\theta + (5/2)\Phi_2(1/2)(3\cos^2\theta - 1)$.
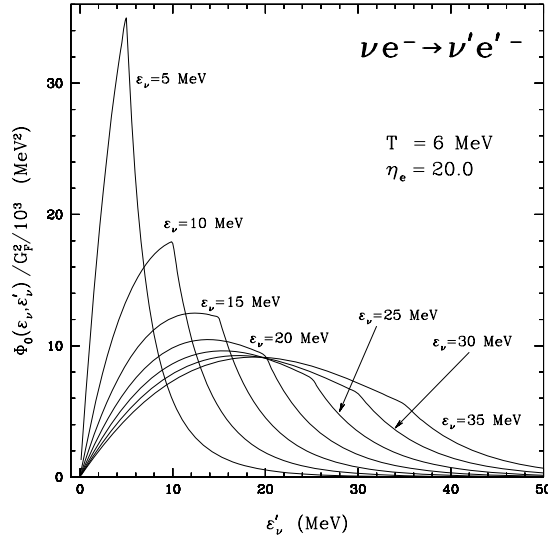
Fig. 3. The $l = 0$ term in the Legendre expansion of the ν_e–electron scattering kernel, $\Phi_0(\varepsilon_\nu, \varepsilon'_\nu)$ (Eq. (37)), for $T = 6$ MeV and $\eta_e = 20$ as a function of ε'_ν for $\varepsilon_\nu = 5$, 10, 15, 20, 25, and 35 MeV. Note that for any ε_ν, the neutrino is predominantly downscattered. The magnitude of $\Phi_0(\varepsilon_\nu, \varepsilon'_\nu)$ and sign of $\langle \omega \rangle$ are to be compared with those in Fig. 5 for ν–nucleon scattering.

A simple approach to handling energy redistribution involves calculating angle and energy moments and deriving source and sink terms (Eqs. (33) and (34); [66]). Substituting into the first term on the right-hand-side of Eq. (33) (the source) gives

$$\tilde{\eta}_\nu^{\text{scatt}} = (1 - f_\nu) \int\limits_0^\infty \frac{d\varepsilon'_\nu \varepsilon'^2_\nu}{c(2\pi\hbar c)^3} e^{-\beta\omega} \int\limits_{-1}^{+1} d\mu' f'_\nu \int\limits_0^{2\pi} d\phi' \left[\frac{1}{2}\Phi_0 + \frac{3}{2}\Phi_1 \cos\theta \right]. \tag{39}$$

Substituting for $\cos\theta$ using Eq. (35) and using the definitions

$$\tilde{J}_\nu = \frac{1}{2} \int\limits_{-1}^{+1} d\mu \, f_\nu \tag{40}$$

and

$$\tilde{H}_\nu = \frac{1}{2} \int\limits_{-1}^{+1} d\mu \, \mu f_\nu \tag{41}$$

we have that

$$\tilde{\eta}_\nu^{\text{scatt}} = (1 - f_\nu) \frac{4\pi}{c(2\pi\hbar c)^3} \int\limits_0^\infty d\varepsilon'_\nu \varepsilon'^2_\nu e^{-\beta\omega} \left[\frac{1}{2}\Phi_0 \tilde{J}'_\nu + \frac{3}{2}\Phi_1 \mu \tilde{H}'_\nu \right]. \tag{42}$$
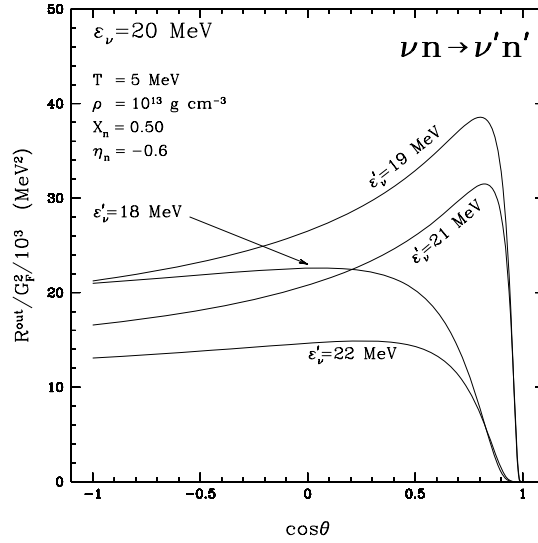
Fig. 4. The scattering kernel $R^{\text{out}}(\varepsilon_\nu, \varepsilon'_\nu, \cos\theta)$ for ν_e–neutron scattering as a function of $\cos\theta$ for $\varepsilon_\nu = 20$ MeV and $\varepsilon'_\nu = 18$, 19, 21, and 22 MeV, at a representative thermodynamic point ($T = 5$ MeV, $\rho = 10^{13}$ g cm^{-3}, $X_n = 0.5$). Note that although the absolute value of the energy transfer ($|\varepsilon_\nu - \varepsilon'_\nu|$) is the same for both $\varepsilon'_\nu = 19$ MeV and $\varepsilon'_\nu = 21$, the absolute value of $R^{\text{out}}(20, 19, \cos\theta)$ is greater than that of $R^{\text{out}}(20, 21, \cos\theta)$, reflecting the fact that at this temperature the incoming neutrino is more likely to downscatter than upscatter.
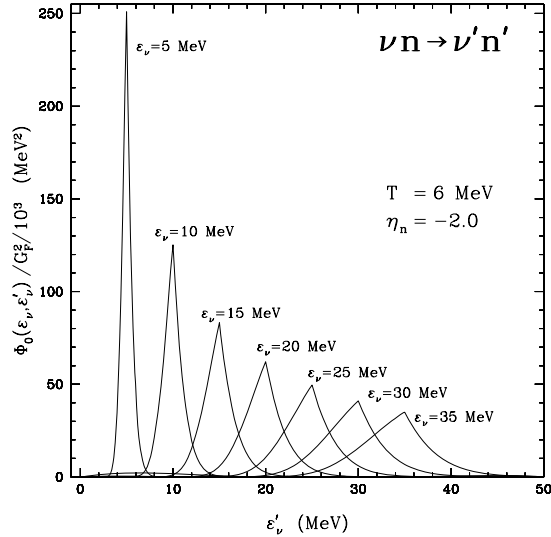

Fig. 5. The $l = 0$ term in the Legendre expansion of the neutrino–nucleon scattering kernel, $\Phi_0(\varepsilon_\nu, \varepsilon'_\nu)$ (Eq. (37)), for $T = 6$ MeV and $\eta_n = -2$ as a function of ε'_ν for $\varepsilon_\nu = 5$, 10, 15, 20, 25, and 35 MeV. Note that for $\varepsilon_\nu = 5$ MeV the neutrino is predominantly upscattered, while for $\varepsilon_\nu = 35$ MeV the neutrino is predominantly downscattered. The magnitude of $\Phi_0(\varepsilon_\nu, \varepsilon'_\nu)$ and sign of $\langle\omega\rangle$ are to be compared with those in Fig. 3.

Integrating over μ to get the source for the zeroth moment of the transport equation,

$$\frac{1}{2}\int_{-1}^{+1} d\mu\, \tilde{\eta}_\nu^{\text{scatt}} = \frac{4\pi}{c(2\pi\hbar c)^3}\int_0^\infty d\varepsilon_\nu'\, \varepsilon_\nu'^2 e^{-\beta\omega}\left[\frac{1}{2}\Phi_0\tilde{J}_\nu'(1-\tilde{J}_\nu) - \frac{3}{2}\Phi_1\tilde{H}_\nu\tilde{H}_\nu'\right]. \qquad (43)$$

Similarly, we can write the sink term of the Boltzmann equation collision term (second term in Eq. (33)), employing the Legendre expansion

$$\tilde{\chi}_\nu^{\text{scatt}} = \frac{4\pi}{c(2\pi\hbar c)^3}\int_0^\infty d\varepsilon_\nu'\, \varepsilon_\nu'^2\left[\frac{1}{2}\Phi_0(1-\tilde{J}_\nu') - \frac{3}{2}\Phi_1\mu\tilde{H}_\nu'\right]. \qquad (44)$$

The contribution to the zeroth moment equation is then

$$\frac{1}{2}\int_{-1}^{+1} d\mu\,(-\tilde{\chi}_\nu^{\text{scatt}} f_\nu)$$

$$= -\frac{4\pi}{c(2\pi\hbar c)^3}\int_0^\infty d\varepsilon_\nu'\, \varepsilon_\nu'^2\left[\frac{1}{2}\Phi_0(1-\tilde{J}_\nu')\tilde{J}_\nu - \frac{3}{2}\Phi_1\tilde{H}_\nu\tilde{H}_\nu'\right]. \qquad (45)$$

Combining these equations, we find that

$$\frac{1}{2}\int_{-1}^{+1} d\mu\, \mathcal{L}_\nu^{\text{scatt}}[f_\nu]$$

$$= \frac{4\pi}{c(2\pi\hbar c)^3}\int_0^\infty d\varepsilon_\nu'\, \varepsilon_\nu'^2\left\{\frac{1}{2}\Phi_0\left[\tilde{J}_\nu'(1-\tilde{J}_\nu)e^{-\beta\omega} - (1-\tilde{J}_\nu')\tilde{J}_\nu\right]\right.$$

$$\left. - \frac{3}{2}\Phi_1\tilde{H}_\nu\tilde{H}_\nu'\left(e^{-\beta\omega}-1\right)\right\}. \qquad (46)$$

One can see immediately that including another term in the Legendre expansion (taking $R^{\text{out}} \sim (1/2)\Phi_0 + (3/2)\Phi_1\cos\theta + (5/2)\Phi_2(1/2)(3\cos^2\theta - 1)$) necessitates including $\tilde{P}_\nu$ and $\tilde{P}_\nu'$, the second angular moment of the neutrino phase-space distribution function, in the source and sink terms. While easily doable, we advocate retaining only the linear term.

5. Inelastic neutrino interactions with relativistic nucleons and leptons

We now explore more sophisticated formalisms for handling inelastic scattering processes in nuclear matter. In this section, we address the non-interacting nucleon case.

For neutrino energies of interest to supernova, which are less than a few hundred MeV, we may write the neutrino–matter interaction in terms of Fermi's effective Lagrangian

Table 1
Neutral and charged current vector, axial and tensor coupling constants. The axial coupling $g_A = -1.23$, the weak mixing angle $\sin^2\theta_W = 0.23$. $\mu_n = -1.913$ and $\mu_p = 1.793$ are the anomalous magnetic moments of the neutron and proton, respectively and $\delta = (\mu_p - \mu_n)/2 = 1.853$

Reaction	c_V, g_V	c_A, g_A	F_2
$\nu_i + n \to \nu_i + n$	$-1/2$	$-g_A/2$	$-2\mu_n \sin^2\theta_W - \delta$
$\nu_i + p \to \nu_i + p$	$1/2 - 2\sin^2\theta_W$	$g_A/2$	$-2\mu_p \sin^2\theta_W + \delta$
$\nu_e + e^- \to \nu_e + e^-$	$1/2 + 2\sin^2\theta_W$	$-1/2$	0
$\nu_{\mu/\tau} + e^- \to \nu_{\mu/\tau} + e^-$	$-1/2 + 2\sin^2\theta_W$	$-1/2$	0
$\nu_e + n \leftrightarrow e^- + p$	1	g_A	2δ

$$\mathcal{L}_{\text{int}}^{cc} = \frac{G_F \cos(\theta_C)}{\sqrt{2}} l_\mu j_W^\mu \quad \text{for } \nu_l + B_2 \to l + B_4, \tag{47}$$

$$\mathcal{L}_{\text{int}}^{nc} = \frac{G_F}{\sqrt{2}} l_\mu^\nu j_Z^\mu \quad \text{for } \nu_l + B_2 \to \nu_l + B_4, \tag{48}$$

where again $G_F \simeq 1.436 \times 10^{-49}$ erg cm^{-3} is the Fermi weak coupling constant and θ_C is the Cabibbo angle. When the typical energy and momentum involved in the reaction are small (compared to the mass and $1/\text{size}$ of the target particle) the lepton and baryon weak charged currents are:

$$l_\mu = \bar{\psi}_l \gamma_\mu (1 - \gamma_5) \psi_\nu, \qquad j_W^\mu = \bar{\psi}_4 \gamma^\mu (g_V - g_A \gamma_5) \psi_2. \tag{49}$$

Similarly, the baryon and neutrino neutral currents are given by

$$l_\mu^\nu = \bar{\psi}_\nu \gamma_\mu (1 - \gamma_5) \psi_\nu, \qquad j_Z^\mu = \bar{\psi}_4 \gamma^\mu (c_V - c_A \gamma_5) \psi_2, \tag{50}$$

where 2 and 4 are the baryon (or electron) initial state and final state labels, respectively (these are identical for neutral-current reactions). The vector and axial-vector coupling constants (c_V, g_V and c_A, g_A) are listed in Table 1 for the various charged- and neutral-current reactions of interest. The charged-current reactions are kinematically suppressed for ν_μ and ν_τ neutrinos. This is because their energy $E_{\nu_\mu/\nu_\tau} \simeq T \leqslant m_\mu, m_\tau$. On the other hand, neutral-current reactions are common to all neutrino species and the neutrino–baryon couplings are independent of neutrino flavor. Neutrino coupling to the lepton in the same family is modified since the scattering may proceed due to both W and Z exchange; the couplings shown in Table 1 reflect this fact.

From the structure of the current–current Lagrangian, we can calculate the differential cross section for neutrino scattering and absorption. We are generally interested in calculating scattering/absorption rates in matter. Hence, it is convenient to express results in terms of the differential scattering/absorption rate. For a neutrino with energy E_1, this is given by $d\Gamma(E_1) = \sum_i c \, d\sigma(E_1)_i / V$, where $d\sigma$ is the differential cross section, the sum is over the target particle in volume V, and $c = 1$ is the (relative) velocity of the neutrinos. For reasons that will soon become clear, it is useful to express the differential rate in terms of the current–current correlation function for the target particles (also called medium polarization tensor and is related to the dynamic structure factor) rather than the S-matrix element involving free asymptotic states.

The differential scattering rate of matter is given by [31,59]:

$$\frac{d\Gamma(E_1)}{d^2\Omega_3\,dE_3} = -\frac{G_F^2}{32\pi^3}\frac{E_3}{E_1}\frac{[1 - f_3(E_3)]}{\left[1 - \exp\left(\frac{-\omega - (\mu_2 - \mu_4)}{T}\right)\right]}\,\mathrm{Im}\left[L^{\alpha\beta}\Pi_{\alpha\beta}^R\right], \tag{51}$$

where the incoming neutrino energy is E_1, the outgoing neutrino (or electron) energy is E_3, and $\omega = E_1 - E_3$. The factor $[1 - \exp((-\omega - \mu_2 + \mu_4)/T)]$ arises due to the fluctuation–dissipation theorem, since particles labeled '2' and '4' are in thermal equilibrium at temperature T and in chemical equilibrium with chemical potentials μ_2 and μ_4, respectively. For neutral-current processes, $\mu_4 = \mu_2$, and for charged-current processes, such as $\nu_e + n \to e^- + p$, $\mu_2 = \mu_n$ and $\mu_4 = \mu_p$. Note also that for charged-current reactions involving nucleons Eq. (51) must be multiplied by a factor of $\cos^2(\theta_C)$. The final-state Pauli blocking of the outgoing lepton is accounted for by the factor $(1 - f_3(E_3))$. The lepton tensor $L_{\alpha\beta}$ is given by

$$L^{\alpha\beta} = 8\left[2k^\alpha k^\beta + (k \cdot q)g^{\alpha\beta} - \left(k^\alpha q^\beta + q^\alpha k^\beta\right) \mp i\epsilon^{\alpha\beta\mu\nu}k_\mu q_\nu\right], \tag{52}$$

where the sign of the last term is positive for anti-neutrinos and negative for neutrinos.

The medium or target particle retarded polarization tensor is given by

$$\mathrm{Im}\,\Pi_{\alpha\beta}^R = \tanh\left(\frac{\omega + (\mu_2 - \mu_4)}{2T}\right)\mathrm{Im}\,\Pi_{\alpha\beta}, \tag{53}$$

where $\Pi_{\alpha\beta}$ is the time-ordered or causal polarization and is given by

$$\Pi_{\alpha\beta} = -i\int\frac{d^4p}{(2\pi)^4}\,\mathrm{Tr}\left[T\left(G_2(p)\Gamma_\alpha G_4(p + q)\Gamma_\beta\right)\right]. \tag{54}$$

Above, k_μ is the incoming neutrino four-momentum and q_μ is the four-momentum transfer. In writing the lepton tensor, we have neglected the electron mass term, since typical electron energies are of the order of a hundred MeV at high densities. The Green's functions $G_i(p)$ (the index i labels particle species) describe the propagation of baryons at finite density and temperature. In a Fermi gas, the fermion Green's function is given by

$$G(p) = \frac{1}{\not{p} + \mu\gamma_0 - m}, \tag{55}$$

where μ is the chemical potential and m is the mass. For the neutral (charged) current, the vertex function Γ_μ is $c_V(g_V)\gamma_\mu$ for the vector current and $c_A(g_A)\gamma_\mu\gamma_5$ for the axial current. Given the structure of the particle currents, we have

$$\Pi_{\alpha\beta} = c_V^2\Pi_{\alpha\beta}^V + c_A^2\Pi_{\alpha\beta}^A + 2c_V c_A\Pi_{\alpha\beta}^{VA}. \tag{56}$$

For the neutral–current, the vector polarization $\Pi_{\alpha,\beta}^V$ is obtained by substituting $\{\Gamma_\alpha, \Gamma_\beta\} :: \{\gamma_\alpha, \gamma_\beta\}$; the axial polarization $\Pi_{\alpha,\beta}^A$ is obtained by substituting $\{\Gamma_\alpha, \Gamma_\beta\} :: \{\gamma_\alpha\gamma_5, \gamma_\beta\gamma_5\}$; and the mixed part $\Pi_{\alpha,\beta}^{VA}$ is obtained by substituting $\{\Gamma_\alpha, \Gamma_\beta\} :: \{\gamma_\alpha\gamma_5, \gamma_\beta\}$.

Using vector current conservation and translational invariance, $\Pi_{\alpha\beta}^V$ may be written in terms of two independent components. In a frame where $q_\mu = (\omega, |q|, 0, 0)$, we have

$$\Pi_T = \Pi_{22}^V \quad\text{and}\quad \Pi_L = -\frac{q_\mu^2}{|q|^2}\Pi_{00}^V.$$

The axial current–current correlation function can be written as a vector piece plus a correction term:

$$\Pi_{\mu\nu}^A = \Pi_{\mu\nu}^V + g_{\mu\nu}\Pi^A. \tag{57}$$

The mixed, axial-current/vector-current correlation function is

$$\Pi_{\mu\nu}^{VA} = i\epsilon_{\mu,\nu,\alpha,0}q^\alpha \Pi^{VA}. \tag{58}$$

These simplifications enable us to write the differential rate in Eq. (51), as follows

$$\frac{d\Gamma}{d^2\Omega\,dE_3} = \frac{G_F^2}{4\pi^3}\frac{E_3}{E_1}q_\mu^2\big[1 - f_3(E_3)\big]\big[A S_1(|\vec{q}|,\omega) + S_2(|\vec{q}|,\omega) \pm B S_3(|\vec{q}|,\omega)\big],$$
$$A = \frac{4E_1 E_3 + q_\mu^2}{2q^2}, \qquad B = E_1 + E_3, \tag{59}$$

where the plus is for neutrinos and the minus is for anti-neutrinos. The three response functions, S_1, S_2, and S_3 are given by

$$S_1(|\vec{q}|,\omega) = \frac{(c_V^2 + c_A^2)(\operatorname{Im}\Pi_L^R(q,\omega) + \operatorname{Im}\Pi_T^R(q,\omega))}{1 - \exp(-\beta(\omega + \mu_2 - \mu_4))}, \tag{60}$$

$$S_2(|\vec{q}|,\omega) = \frac{(c_V^2 + c_A^2)\operatorname{Im}\Pi_T^R(q,\omega) - c_A^2 \operatorname{Im}\Pi_A^R(q,\omega)}{1 - \exp(-\beta(\omega + \mu_2 - \mu_4))}, \tag{61}$$

$$S_3(|\vec{q}|,\omega) = \frac{2c_V c_A \operatorname{Im}\Pi_{VA}^R(q,\omega)}{1 - \exp(-\beta(\omega + \mu_2 - \mu_4))}. \tag{62}$$

The imaginary parts of the polarization functions needed to evaluate the response functions have been calculated explicitly by Horowitz and Wehrberger [31,32] and Reddy et al. [60]. Neutrino scattering and absorption kinematics probes space-like kinematics where $q_\mu^2 \leqslant 0$ (this is true only for massless neutrinos and electrons; however, when the typical lepton energies are large compared to m_e, restriction to space-like kinematics is a good approximation). For space-like excitations,

$$\operatorname{Im}\Pi_L^R(q,\omega) = \frac{q_\mu^2}{2\pi|q|^3}\left[I_2 + \omega I_1 + \frac{q_\mu^2}{4}I_0\right], \tag{63}$$

$$\operatorname{Im}\Pi_T^R(q,\omega) = \frac{q_\mu^2}{4\pi|q|^3}\left[I_2 + \omega I_1 + \left(\frac{q_\mu^2}{4} + \frac{q^2}{2} + M_2^2\frac{q^2}{q_\mu^2}\right)I_0\right], \tag{64}$$

$$\operatorname{Im}\Pi_A^R(q,\omega) = \frac{M_2^2}{2\pi|q|}I_0, \tag{65}$$

$$\operatorname{Im}\Pi_{VA}^R(q,\omega) = \frac{q_\mu^2}{8\pi|q|^3}[\omega I_0 + 2I_1], \tag{66}$$

where M_i is the rest mass of particle i. The one-dimensional integrals

$$I_n = \tanh\left(\frac{\omega + (\mu_2 - \mu_4)}{2T}\right)\int_{e_-}^{\infty} dE\, E^n\big[F(E, E + \omega) + F(E + \omega, E)\big], \tag{67}$$

where $F(x, y) = f_2(x)(1 - f_4(y))$ and $f_i(E)$ are Fermi–Dirac particle distribution functions. The lower limit on the integral, e_-, arises due to kinematical restrictions and is given by

$$e_- = -\beta \frac{\omega}{2} + \frac{q}{2} \sqrt{\beta^2 - 4 \frac{M_2^2}{q^2 - \omega^2}}, \tag{68}$$

where

$$\beta = 1 + \frac{M_4^2 - M_2^2}{q^2 - \omega^2}. \tag{69}$$

These integrals may be explicitly expressed in terms of the polylogarithmic functions

$$\mathrm{Li}_n(z) = \int\limits_0^z \frac{\mathrm{Li}_{n-1}(x)}{x} dx, \qquad \mathrm{Li}_1(x) = \ln(1 - x). \tag{70}$$

This polylogarithm representation is particularly useful and compact:

$$I_0 = Tz \left(1 + \frac{\xi_1}{z} \right), \tag{71}$$

$$I_1 = T^2 z \left(\frac{\mu_2 - U_2}{T} - \frac{z}{2} + \frac{\xi_2}{z} + \frac{e_- \xi_1}{zT} \right), \tag{72}$$

$$I_2 = T^3 z \left(\frac{(\mu_2 - U_2)^2}{T^2} - z \frac{\mu_2 - U_2}{T} + \frac{\pi^2}{3} + \frac{z^2}{3} - 2 \frac{\xi_3}{z} + 2 \frac{e_- \xi_2}{Tz} + \frac{e_-^2 \xi_1}{T^2 z} \right), \tag{73}$$

where $z = (\omega + (\mu_2 - \mu_4))/T$ and the factors ξ_n are given by

$$\xi_n = \mathrm{Li}_n(-\alpha_1) - \mathrm{Li}_n(-\alpha_2), \tag{74}$$

with

$$\alpha_1 = \exp\big((e_- - \mu_2)/T\big), \qquad \alpha_2 = \exp\big((e_- + \omega - \mu_4)/T\big). \tag{75}$$

In the case of neutral currents, some of the terms above simplify

$$z = \frac{\omega}{T}, \qquad \mu_2 = \mu_4, \qquad e_- = -\frac{\omega}{2} + \frac{q}{2} \sqrt{1 - 4 \frac{M_2^{*2}}{q_\mu^2}}. \tag{76}$$

The total scattering rate is the double integral in (q, ω) space:

$$\Gamma = \frac{G_{\mathrm{F}}^2}{2\pi^2 E_1^2} \int\limits_{-\infty}^{E_1} d\omega \left(1 - f_3(E_3) \right) \int\limits_{|\omega|}^{2E_1 - \omega} dq \, q q_\mu^2 [AS_1 + S_2 \pm BS_3]. \tag{77}$$

Eq. (77) allows us to calculate the cross section per unit volume, or equivalently the inverse mean free path. This naturally incorporates the effects of Pauli blocking, Fermi and thermal motion of target particles, and the contribution of relativistic terms to the electron and baryon currents. The formalism reviewed in this section provides a unified description of reactions (both charged and neutral currents) involving both nucleons and electrons. In

the absence of strong and electromagnetic interactions, this is almost all there is to the subject of neutrino opacities in matter with nucleons and leptons. The only omission here is the effect of weak magnetism (Section 3.1). This arises due to tensor coupling between neutrinos and nucleons and is discussed next.

The vector and axial-vector structure of the weak hadronic currents given in Eqs. (49) and (50) are valid only at low energy ($E_\nu \ll M$). When the neutrino energy becomes comparable to the intrinsic energy scale that characterizes the hadron (its size and mass) additional contributions arise. These include form factors and the tensor (weak magnetism) couplings. To leading order in the four-momentum transfer expansion (q_μ), the hadronic neutral and charged weak currents take the form

$$j_W^\mu = \bar{\psi}_4 \left[g_V(q_\mu^2)\gamma^\mu + i F_2(q_\mu^2)\sigma^{\mu\nu}\frac{q_\nu}{2M} - g_A(q_\mu^2)\gamma^\mu\gamma_5 \right]\psi_2, \tag{78}$$

$$j_Z^\mu = \bar{\psi}_4 \left[c_V^i(q_\mu^2)\gamma^\mu - i F_2^i(q_\mu^2)\sigma^{\mu\nu}\frac{q_\nu}{2M} - c_A^i(q_\mu^2)\gamma^\mu\gamma_5 \right]\psi_2. \tag{79}$$

The q_μ^2 dependence of the vector and axial couplings is weak and one can safely ignore these corrections, but the contribution from weak magnetism is not negligible [68]. The tensor coupling constants for the various reactions of interest are given in Table 1. For a neutrino of energy $E_\nu \simeq 50$ MeV, a typical $|\vec{q}| \sim 2E_\nu \sim 100$ MeV, the weak magnetism correction to the vector current is then $F_2|\vec{q}|/(2M) \simeq 6\%$. Perhaps, more importantly, these corrections appear with opposite sign for neutrinos and anti-neutrinos [34,68], resulting in 10–20% differences in the relative cross sections.

Tensor coupling introduces new structure to the current–current correlation function given in Eq. (56) and corresponding changes to the response functions given in Eq. (62). These corrections have been computed in recent work by Horowitz and Pérez-García [35]. To order q^2/M, the tensor–vector, tensor–axial vector and tensor–tensor polarization functions contribute to the neutrino response. These are obtained from Eq. (54), with the following substitutions: for the tensor–vector, $\Gamma_\alpha = i F_2 \sigma_{\alpha,\delta} q^\delta/2M$ and $\Gamma_\beta = c_v \gamma_\beta$; for the tensor–axial, $\Gamma_\alpha = i F_2 \sigma_{\alpha,\delta} q^\delta/2M$ and $\Gamma_\beta = c_a \gamma_\beta \gamma_5$; and for the tensor–tensor, $\Gamma_\alpha = i F_2 \sigma_{\alpha,\delta} q^\delta/2M$ and $\Gamma_\beta = i F_2 \sigma_{\beta,\delta} q^\delta/2M$. These polarization functions can be related to the vector, axial, and vector–axial polarization tensors discussed earlier. Explicit forms for the imaginary parts of these polarization tensors can be found in [35].

6. Strong and electromagnetic correlations between nuclei, nucleons, and electrons

The results of the previous sections provide a complete description of neutrino cross sections in an ideal Fermi gas of nucleons and leptons. Here, we address non-ideal corrections to neutrino scattering rates arising due to interactions between nucleons, electrons and nuclei. The role of correlations in neutrino opacities was first appreciated in the pioneering works of Sawyer [61] and Iwamoto and Pethick [37]. They showed that strong interactions between nucleons could significantly modify (by as much as a factor of 2–3) neutrino cross sections at densities and temperatures of relevance to supernovae. In the past decade, there have been several attempts to incorporate these effects in calculations of the neutrino

opacity of dense matter. While much progress has been made in understanding qualitative aspects of these corrections, quantitative predictions for the neutrino cross sections at high density remain elusive. We present a pedagogic review of the qualitative findings of model calculations, provide an overview of the current state of the art of many-body effects in neutrino cross sections, and comment on their shortcomings.

6.1. Plasma of heavy ions: neutrino opacity at $\rho \sim 10^{12}$ g/cm³

The simplest system, with non-trivial many-body dynamics, which is relevant in the supernova context is a plasma of heavy nuclei (like Fe) immersed in a background of degenerate electrons. Freedman [21] showed that the dominant source of opacity for neutrinos in such a plasma is the coherent scattering off nuclei. Low-energy neutrinos can couple coherently, via the vector neutral current, to the total weak charge of the nucleus. The weak charge of a nucleus with A nucleons and Z protons is given by $Q_W = (2Z - A - 4Z \sin^2 \theta_W)/2$.

For neutrino–nucleus scattering in a plasma, we must properly account for the presence of other nuclei, since scattering from these different sources can interfere. In the language of many-body theory, this screening is encoded in the density–density correlation function. It is therefore natural to express the scattering rate in terms of these correlation functions as described earlier in Section 5. To motivate the relation between the cross section and the density–density correlation function we begin by noting that the effective Lagrangian describing the neutral-current interaction of low-energy neutrinos with nuclei is given by

$$L_{NC} = \frac{G_F}{\sqrt{2}} Q_W l_\mu j^\mu \tag{80}$$

where $l_\mu = \bar{\nu} \gamma_\mu (1 - \gamma_5) \nu$ is the neutrino neutral current. Nuclei are heavy, and, correspondingly, their thermal velocities are small ($v \cong \sqrt{T/M} \ll c$). For simplicity, we assume that nuclei are bosons characterized only by their charge and baryon number. In this case it is an excellent approximation to write the neutral current carried by the nuclei as $j^\mu = \psi^\dagger \psi \delta_0^\mu$. We can write the differential scattering rate in terms of the density operator in momentum space given by

$$\rho(\vec{q}, t) = \psi^\dagger \psi = \sum_{i=1,\dots,N} \exp(i\vec{q} \cdot \vec{r}_i(t)), \tag{81}$$

where the sum is over N particles in a volume V which are labeled $i = 1, \dots, N$. The rate for scattering of a neutrino with energy E_ν to a state with energy $E'_\nu = E_\nu - \omega$, at an angle θ, with a momentum transfer $\vec{q}$ is given by

$$\frac{d\Gamma}{d\cos\theta \, dE'_\nu} = \frac{G_F^2}{4\pi^2} Q_W^2 (1 + \cos\theta) E'^2_\nu S(|\vec{q}|, \omega). \tag{82}$$

The function $S(|\vec{q}|, \omega)$ is called the dynamic structure function. It embodies all spatial and temporal correlations between target particles arising from strong or electromagnetic interactions and is given by

$$S(|\vec{q}|, \omega) = \int_{-\infty}^{\infty} dt \exp(i\omega t) \langle \rho(\vec{q}, t) \rho(-\vec{q}, 0) \rangle. \tag{83}$$

In the above, $\langle\cdots\rangle$ denotes the ensemble average per unit volume. Note that $S(|\vec{q}|, \omega)$ is normalized such that in the elastic limit for a non-degenerate, non-interacting gas $S(|\vec{q}|, \omega) = 2\pi\delta(\omega)n$, where $n = N/V$ is the density of particles.

To calculate the structure function we need to solve for the dynamics ($\vec{r}(t)$) of the ions as they move in each others presence, interacting via the two-body ion–ion interaction potential. The electrons are relativistic and degenerate, and the electron Fermi momentum $k_{\rm F} = (3\pi^2 Zn)^{1/3}$. The timescale associated with changes in their density distribution is rapid compared to the slow changes we expect in the density field of the heavy ions. Electrons almost "instantaneously" follow the ions and screen the Coulomb potential between ions. Correspondingly, there is small excess in the electron distribution around each ion. As first discussed by Leinson et al. [43], this excess will also screen the weak charge of the nucleus to which the neutrinos couple. Electronic screening was discussed earlier in Section 3.6 and Eq. (25). Here, we focus on the dynamics of ions interacting through the screened potential $V(r) = Z^2 e^2 \exp(-r/\lambda_e)/(4\pi r)$, where $\lambda_e = \sqrt{4\alpha_{\rm em}/\pi}\, k_{\rm F}^{-1}$ is the electron Debye screening length.

At 10^{12} g/cm^3, the typical inter-ion distance is $d \lesssim 30$ fm, $\lambda_e \geqslant 80$ fm, and the typical ion–ion interaction energy, $E_{\rm pot} \simeq Z^2 e^2/(4\pi d)$, is large. For temperature in the range 1–5 MeV, the ratio of the potential energy to the kinetic energy, Γ, equals $Z^2\alpha_{\rm em}/(dkT)$. For nickel-like nuclei with $Z = 28$, $\Gamma = 8.8$ for $T = 4$ MeV. The dynamics of such a strongly coupled plasma is not amenable to analytic methods of perturbation theory and approximate non-perturbative methods have had limited success in describing these systems. For a classical system of point particles interacting via a 2-body potential it is possible to numerically simulate the real-time dynamics of the system. Such simulations confine N particles to a box with periodic boundary conditions, calculate the force on each particle at any time, and evolve the particles by using their equations of motion ($\ddot{\vec{r}} = {\rm Force}/M$, where M is the mass of the ion). This technique, which goes by the name molecular dynamics (MD), has been used extensively in condensed matter physics, plasma physics, and chemistry. For an early application of this technique to the study of the response of a one-component plasma (see [29]).

The de Broglie wavelength of the ions is $\Lambda_{\rm D} \simeq 4.6 \times A^{-1} T_{\rm MeV}^{-1}$ fm, where A is the mass number of the ion and $T_{\rm MeV}$ is the temperature in MeV. For $T \geqslant 1$ MeV, $\Lambda_{\rm D} \ll d$, the ion–plasma is classical, and we may implement MD to calculate $S(|\vec{q}|, \omega)$. Fig. 6 shows the results of such a calculation (from [47]). We chose to simulate 54 ions ($A = 56$, $Z = 28$) in a box of length $L = 200$ fm. This corresponds to an ion density $n = 6.75 \times 10^{-6}$ fm^{-3} or the mass density $\rho \approx 6 \times 10^{12}$ g/cm^3. The background electron density was chosen to make the system electrically neutral. For a classical simulation, the system is characterized by the plasma Γ defined earlier. Fig. 6 shows a comparison between the results for $S(\vec{q}, \omega)$ obtained by MD simulations (dots with error bars), the free (Boltzmann) gas response (dashed-line), and the response obtained using Random Phase Approximation (RPA). The response in RPA is discussed in the next section. The results are shown as a function of $\omega/\omega_{\rm plasmon}$, where ω is the energy transfer, and $\omega_{\rm plasmon} = \sqrt{4\pi\alpha_{\rm em}n/M}$ is the plasma frequency of the classical heavy-ion plasma.

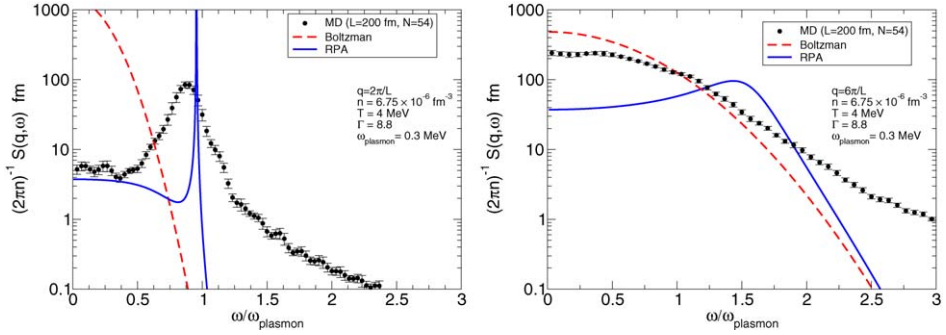Fig. 6. Dynamic structure function of a plasma of ions as a function of energy transfer ω (measured in units of the plasma frequency $\omega_p \simeq 0.3$ MeV) and fixed momentum transfer $|\vec{q}| = 2\pi/L \simeq 6$ MeV (left panel) and $|\vec{q}| = 6\pi/L \simeq 18$ MeV (right panel). Statistical errors for the results of the molecular dynamics simulations are also indicated.

6.1.1. Random phase approximation (RPA)

We motivate and present a heuristic derivation of the structure function calculated using the random phase approximation. To begin, we note that the dynamic structure factor for a non-relativistic and non-interacting Maxwell–Boltzmann gas with a chemical potential μ_A and number density n is given by

$$S_{\mathrm{MB}}(\vec{q}, \omega) = \int \frac{d^3 p}{(2\pi)^3} f(E_{\vec{p}}) 2\pi \delta(E_{\vec{p}} - E_{\vec{p}+\vec{q}} + \omega)$$

$$= \frac{n}{q} \sqrt{\frac{2\pi M}{kT}} \exp\left(-Q_+^2\right), \tag{84}$$

where

$$Q_+^2 = \frac{M}{2kT}\left(-\frac{\omega}{q} + \frac{q}{2M}\right)^2, \tag{85}$$

and

$$n = \left(\frac{MkT}{2\pi}\right)^{3/2} \exp\left(\frac{\mu_A}{kT}\right). \tag{86}$$

This follows directly from the equation of motion of the free particles and Eq. (83). When an external current couples to the interacting system at wavelengths large compared to the inter-particle spacing, scattering amplitudes from different particles can interfere. In the case of neutrino scattering this leads to screening of the weak charge. RPA is known to provide an adequate description of this dynamic screening in the long-wavelength limit. Pioneering work by Bohm and Pines [4] established RPA as a useful non-perturbative approximation. It is used widely in nuclear and solid state physics to describe the long-wavelength response of many-particle systems. In particular, RPA accounts for dynamic screening and is able to correctly predict the presence of collective modes. These correspond to a plasmon in the case of unscreened Coulomb interactions and phonons in the case of screened interactions (as in the present case). The RPA results in Fig. 6 clearly show the presence of these collective states.
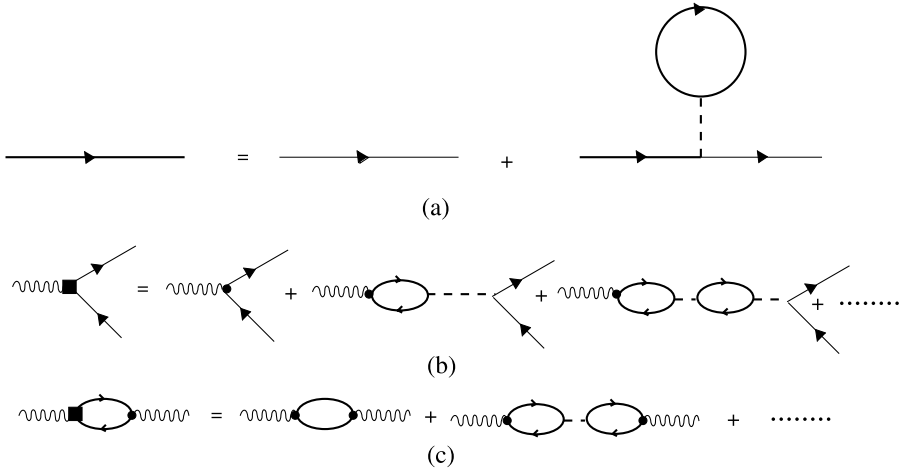
Fig. 7. Feynman diagram representing the Schwinger–Dyson equations: (a) mean field (Hartree) propogator; (b) dressed vertex for coupling to an external current with in the RPA; and (c) RPA polarization tensor or current–current correlation function for the coupling to external currents. Dressed propagators are thick solid lines, bare propagators are thin lines, dashed lines are strong/electromagnetic interactions, wavy line is the external (weak) current, the filled circle is the bare weak vertex, and the filled square represents the dressed weak vertex.

Screening in RPA is accounted for by the selective re-summation of an infinite series of bubble graphs. The bubbles are free excitations and are connected by the two-body interaction potential. The lower diagram in Fig. 7 represents this series. The solid lines represent propagation of ions, the wavy line represents the external current (the neutral current), and the dashed lines represent the screened Coulomb interaction. The diagram illustrates screening of the coupling between the external probe (neutrinos in the present case) and particles in the plasma through the intermediate particle–hole excitations. The bubble-sum is a geometric series in the interaction and can be evaluated analytically for simple interactions. For the ion–plasma, the dynamic structure function in RPA is given by

$$S_{\text{RPA}}(\vec{q}, \omega) = \frac{2\hbar}{1 - \exp(-\beta\hbar\omega)} \text{Im}\left[\frac{\Pi_0(\vec{q}, \omega)}{1 - V_{\text{C}}(q)\Pi_0(\vec{q}, \omega)} \right], \tag{87}$$

where

$$V_{\text{C}}(q) = \alpha_{\text{em}} Z^2 \left(\frac{\lambda_e^2}{1 + q^2\lambda_e^2} \right). \tag{88}$$

The expression for $V_{\text{C}}(q)$ is valid for $q \ll k_{\text{F}}$, where λ_e is the Debye screening length and k_{F} is the Fermi momentum of the background degenerate electron gas. The free-gas polarization function

$$\Pi_0(\vec{q}, \omega) = i \int \frac{d^4 p}{(2\pi)^4} G(p)G(p+q), \tag{89}$$

where $G(p) = (p_0 - (p^2/2M - \mu_A))^{-1}$ is the free particle, non-relativistic, Green's function and μ_A is chemical potential of the ions. Analytic expressions for the real and

imaginary parts of Π_0 were first obtained by Lindhard [46]. In the case of a Boltzmann gas these are given by

$$\operatorname{Im}\Pi_0(\vec{q},\omega) = \frac{M^2}{2\pi q\beta}\left(1 - \exp(-\beta\hbar\omega)\right)\exp\left(-Q_+^2\right), \tag{90}$$

$$\operatorname{Re}\Pi_0(\vec{q},\omega) = \mathcal{P}\int \frac{d\omega'}{\pi}\frac{\operatorname{Im}\Pi_0(\vec{q},\omega')}{\omega - \omega'}, \tag{91}$$

where Q_+^2 was defined earlier in Eq. (85).

The comparison in Fig. 6 shows that both RPA and the free-gas response differ quantitatively. MD is exact in the classical limit. Corrections to classical evolution are governed by the smallness of the expansion parameter Λ_{D}/d. In the present case $(\Lambda_{\mathrm{D}}/d) \ll 1\%$. In the left panel, the response for long wavelengths ($|\vec{q}| = 2\pi/L \simeq 6$ MeV) is shown. In this case, the discrepancy between RPA and MD is not significant, supporting the expectation that RPA provides a fair description at long wavelengths. It captures, albeit much too sharply, the phonon peak (which in solid state parlance is called the Bohm–Staver sound) seen in MD simulations. The right panel shows results for $q = 6\pi/L \simeq 18$ MeV. This corresponds to a wavelength that is comparable to the inter-ion distance. Here, the plasmon mode is damped in RPA by single-particle excitations, since $\omega_{\mathrm{plasmon}} \simeq qv_{\mathrm{thermal}}$, where $v_{\mathrm{thermal}} = \sqrt{3kT/M}$ is the thermal velocity of the ions. Nonetheless, this damping is still too weak to dissolve the plasmon peak. In contrast, results obtained using MD do not show any collective behavior, suggesting that RPA underestimates damping.

These results clearly illustrate two important features of the response of strongly-correlated systems:

(1) correlations can greatly affect the shape of the low-energy response; and
(2) approximate many-body methods such as RPA can capture qualitative aspects of the response at large wavelength, but do poorly even at moderate wavelength.

The failure of RPA can be attributed to the neglect of collisional damping from the excitation of multi-particle states. As the ions move, they "simultaneously" scatter off several correlated neighboring particles. In RPA, these correlations are neglected. Ignoring these multi-pair excitations is a reasonable approximation in the long-wavelength limit. We will justify this in our subsequent discussion of sum rules (Section 6.1.2), where we will argue that the spectrum of multi-pair excitations vanishes as q^2 in the $q \to 0$ limit. However, the results indicate significant contribution from multi-pair excitations even at moderate wavelength. Finding ways to incorporate collisional damping of single-particle motion in the response has a long history in solid state physics, starting with the pioneering work of Kadanoff and Martin [40]. We will not review these techniques here. Our focus was to illustrate the importance of many-particle dynamics and provide a baseline for comparison. The lessons learned here will prove valuable in gauging the validity of results that will discussed in Section 6.3, where we evaluate the results obtained using RPA.

6.1.2. Sum rules

The dynamic structure factor is subject to constraints arising due to thermodynamic considerations and symmetries of the Hamiltonian (conservation laws) describing the

many-particle system. These constraints, called sum rules, provide valuable guidance in developing approximation schemes needed to compute $S(|\vec{q}|, \omega)$. In the following, we discuss two such sum rules:

 (i) the compressibility sum rule; and
(ii) the energy-weighted sum rule.

The compressibility sum rule is related to the long-wavelength limit of the static structure function which is defined as

$$S_{|\vec{q}|} = \frac{1}{n} \int\limits_{-\infty}^{\infty} \frac{d\omega}{2\pi} S(|\vec{q}|, \omega). \tag{92}$$

In the long-wavelength limit ($\vec{q} \to 0$), the static structure function is related to the isothermal compressibility by the following relation

$$\lim_{\vec{q} \to 0} S_{|\vec{q}|} = \frac{1}{2\pi n} \lim_{\vec{q} \to 0} \langle \rho(-\vec{q}, 0)\rho(\vec{q}, 0) \rangle = nkT\mathcal{K}_T, \tag{93}$$

where

$$\mathcal{K}_T = -\frac{1}{V}\left(\frac{\partial V}{\partial P}\right)_T \tag{94}$$

is the isothermal compressibility and n is the particle number density. The first of the above relations follows directly from the definition of $S(q, \omega)$ in terms of the density–density correlation function in Eq. (83). The above relation permits us to verify consistency between the neutrino response functions and the equation of state.

The energy-weighted or F sum rule for any operator $\hat{\mathcal{O}}$ is given by

$$\int\limits_{0}^{\infty} \frac{d\omega}{2\pi} \omega \left(\frac{1 - \exp(-\beta\hbar\omega)}{\hbar}\right) S_{\hat{\mathcal{O}}}(\vec{q}, \omega) = \langle[[H, \hat{\mathcal{O}}(\vec{q})], \hat{\mathcal{O}}(\vec{q})]\rangle. \tag{95}$$

In the absence of any velocity-dependent terms in the Hamiltonian, and for the specific case of the density operator, the right hand of Eq. (95) is independent of interactions and is given by

$$\langle[[H, \rho(\vec{q})], \rho(\vec{q})]\rangle = n\frac{q^2}{2M}. \tag{96}$$

Note that the F sum rule vanishes in the long-wavelength limit when the operator $\rho(0)$ commutes with the Hamiltonian. This is a consequence of the conservation of particle number and provides a useful constraint for the large ω behavior of $S(\vec{q}, \omega)$ when it is computed using approximate many-body methods. For the response of the ion–plasma discussed above, the results obtained in the case of the free Boltzmann response, the RPA, and molecular dynamics satisfy this F sum rule. Despite the large differences in the low-energy strength. Another important consequence of the F sum-rule is that it requires response at long wavelengths to vanish as q^2. This implies that multi-particle excitations are suppressed at long wavelength when the operator commutes with the Hamiltonian. It also offers an explanation for the trend seen in Fig. 6, where RPA results improve at large wavelength.

6.2. Pasta phases: neutrino opacity at $\rho \geqslant 10^{13}$ g/cm^3

With increasing density, the nuclei get bigger and the internuclear distance becomes smaller. Under these conditions, the nuclear surface and Coulomb contributions to the free energy of the system become important. Ravenhall et al. [58] showed that it is energetically favorable for nuclei to deform and assume novel, non-spherical, shapes such as rods and slabs. Further, the energy differences between these various shapes are small $\Delta E \simeq 10$–100 keV. The dynamics of such an exotic heterogeneous phase is a complex problem involving several energy scales. Both strong and electromagnetic interactions play an important role. For temperatures of interest, $T \lesssim 5$ MeV, the de Broglie wavelength and the inter-particle distance are comparable and quantum effects cannot be neglected. Recently, Watanabe et al. [69] have studied the behavior of such matter using the techniques of quantum molecular dynamics and also find rod- and slab-like configurations. How does the heterogeneity and existence of several low-energy excitations involving shape fluctuations influence the response of this phase to neutrinos? In the simplest description, the structure size (r) and the inter-structure distance (R) characterize the system. We can expect that neutrinos with wavelength large compared to the structure size, but small compared to the inter-structure distance, can couple coherently to the total weak charge (excess) of the structure, much like the coherence we discussed in the previous section. The effects of this coherent enhancement in the neutrino cross sections has recently been investigated by Horowitz, Pérez-García, Piekarewicz [36]. In agreement with our naive expectation, their study finds that the neutrino cross sections are greatly enhanced, by as much as an order of magnitude, for neutrinos with energy $1/r \geqslant E_\nu \geqslant 1/R$.

6.3. Nuclear liquid: neutrino opacity at $\rho \geqslant 10^{14}$ g/cm^3

When the density of matter exceed 10^{14} g/cm^3, matter is expected to form a homogeneous liquid of nucleons and leptons. To account for the effects of strong and electromagnetic correlations between target neutrons, protons and electrons we must find ways to improve $\Pi_{\alpha\beta}$, the polarization tensor of free Fermi gas described earlier in Eq. (54). This involves improving the Green's functions for the particles and the associated vertex corrections that modify the current operators. In strongly coupled systems, these improvements are notoriously difficult and no exact analytic methods exist. With few exceptions, most investigations of many-body effects in the neutrino opacities have employed the mean-field theory to improve the Green's functions.

Dressing the single particle Green's functions must be accompanied by corresponding corrections to the weak interaction vertex function. The Green's functions in the mean field (Hartree) approximation involves the Schwinger–Dyson summation of the diagrams shown in Fig. 7. The dressing of Green's functions implies the presence of an interaction "cloud" surrounding the quasi-particle. This cloud modifies the coupling of an external probe to the quasi-particle. In Section 6.1, we discussed this screening of the weak charge due to Coulomb interactions between ions within RPA. Here, we consider screening due to both and strong and electromagnetic interactions. The modification of the coupling of an external current to the quasi-particles is shown in the lower panel of Fig. 7, where the solid squares represent interactions between nucleons.

6.3.1. Non-relativistic RPA

At sub-nuclear density, nucleons are non-relativistic. In the non-relativistic limit the structure of the hadronic current greatly simplifies and the vector and axial currents can be directly related to the density and spin-density operators. Neutrino scattering off a non-relativistic neutron liquid was first investigated by Iwamoto and Pethick [37]. In this case, the scattering rate can be written as

$$
\frac{d\Gamma}{d\cos\theta\, dE_\nu'} = \frac{G_F^2}{4\pi^2}\left(1 - f_\nu(E_\nu')\right)E_\nu'^2
$$
$$
\times \left(c_V^2(1+\cos\theta)S\left(|\vec{q}|,\omega\right) + c_A^2(3-\cos\theta)S^A\left(|\vec{q}|,\omega\right)\right),
\tag{97}
$$

where the dynamic structure function for density fluctuations is

$$
S\left(|\vec{q}|,\omega\right) = \int_{-\infty}^{\infty} dt\,\exp(i\omega t)\langle\rho(\vec{q},t)\rho(-\vec{q},0)\rangle,
\tag{98}
$$

and the dynamic structure function for spin-density fluctuations is

$$
S^A\left(|\vec{q}|,\omega\right) = \int_{-\infty}^{\infty} dt\,\exp(i\omega t)\delta_{ij}\langle\sigma_i(\vec{q},t)\sigma(-\vec{q},0)\rangle.
\tag{99}
$$

The thermal ensemble average is denoted by $\langle\cdots\rangle$. It samples the operators over all states of the many-particle system with weight $\exp(-\mathcal{H}/kT)$, where $\mathcal{H}$ is the Hamiltonian describing the neutron liquid. The formalism is easily extended to include protons [13,14,31, 61]. In this case, the differential neutrino–nucleon scattering rate from a liquid of neutrons and protons is given by,

$$
\frac{d^2\Gamma}{d\omega\, d\cos\theta} = \left(4\pi^2\right)^{-1}G_F^2 E_2^2\left[1 - f_\nu(E_2)\right]\left[(1+\cos\theta)\left(c_V^n\right)^2 S_{nn}(q,\omega)\right.
$$
$$
\left. + (3-\cos\theta)g_A^2\left[S_{pp}^A(q,\omega) + S_{nn}^A(q,\omega) - 2S_{pn}^A(q,\omega)\right]\right],
\tag{100}
$$

where $E_2 = E_1 - \omega$.

Following [13], we consider a simple nuclear potential, with only central s-wave interactions, given by

$$
\mathcal{V} = V_1 + V_2\tau_1\cdot\tau_2 + V_3\sigma_1\cdot\sigma_2 + V_4\sigma_1\cdot\sigma_2\tau_1\cdot\tau_2,
\tag{101}
$$

where σ and τ are 2×2 Pauli matrices acting in spin and iso-spin space, respectively. The structure functions, S (Fermi) and S^A (Gamow–Teller; axial), are elements of separate 2×2 symmetric matrices. For the vector dynamic structure function, S, we have

$$
S(q,\omega) = \begin{pmatrix} S_{pp}(q,\omega) & S_{pn}(q,\omega) \\ S_{pn}(q,\omega) & S_{nn}(q,\omega) \end{pmatrix}.
$$

The structure function matrix is given by,

$$
S(q,\omega) = 2\,\mathrm{Im}\left[\Pi^{(0)}(q,\omega)\left[1 - v(q)\Pi^{(0)}(q,\omega)\right]^{-1}\right]\left(1 - e^{-\beta\omega}\right)^{-1},
\tag{102}
$$

where

$$\Pi^{(0)}(q,\omega) = \begin{pmatrix} \Pi_p^{(0)}(q,\omega) & 0 \\ 0 & \Pi_n^{(0)}(q,\omega) \end{pmatrix}$$

and $\Pi_p^{(0)}$ and $\Pi_n^{(0)}$ are given by the Fermi gas polarization functions and evaluated with the proton and neutron chemical potentials, respectively. The non-relativistic polarization for a Fermi gas is given by

$$\operatorname{Im}\Pi^{(0)}(q,\omega) = \frac{m^2}{2\pi q\beta}\log\left[\frac{1+e^{-Q_+^2+\beta\mu}}{1+e^{-Q_+^2+\beta\mu-\beta\omega}}\right], \tag{103}$$

$$\operatorname{Re}\Pi^{(0)}(q,\omega) = \mathcal{P}\int\frac{d\omega'}{\pi}\frac{\operatorname{Im}\Pi^{(0)}(q,\omega)}{\omega-\omega'}, \tag{104}$$

where

$$Q_\pm = \left(\frac{m\beta}{2}\right)^{1/2}\left(\mp\frac{\omega}{q}+\frac{q}{2m}\right). \tag{105}$$

The potential matrix is,

$$v = \begin{pmatrix} v_1+v_2+4\pi e^2(q^2+q_{\mathrm{TF}}^2)^{-1} & v_1-v_2 \\ v_1-v_2 & v_1+v_2 \end{pmatrix},$$

where $v_i = \int d^3r\, V_i$, and the term containing q_{TF} is the Thomas–Fermi screened Coulomb potential ($q_{\mathrm{TF}}^2 = 4e^2\pi^{1/3}(3\bar{n}_p)^{2/3}$). In Fermi liquid theory (FLT), the underlying interaction between (quasi)particle–hole states is directly related to thermodynamic quantities such as the susceptibilities and specific heat (see [3] for a pedagogic introduction to FLT). These effective interactions can differ greatly from the free-space nucleon–nucleon potentials. In the absence of experimental determinations of the thermodynamic susceptibilities, microscopic theories of nuclear interactions are need to obtain these effective interactions. For the simple case of only central interactions, the susceptibilities of nuclear matter are encoded in four constants called Landau parameters (F_0, F_0', G_0, G_0' correspond to baryon density, isospin density, spin-density and spin–isospin density fluctuations, respectively). Following [13,14] and for simplicity, we use these Landau parameters to determine the potential matrix, in lieu of a more developed nuclear interaction model. The parameters of the potential matrix are related to the Landau parameters by the following relations

$$v_1+v_2 = \frac{F_0+F_0'}{N_0}, \qquad v_1-v_2 = \frac{F_0-F_0'}{N_0},$$

$$v_3+v_4 = \frac{G_0+G_0'}{N_0}, \qquad v_3-v_4 = \frac{G_0-G_0'}{N_0},$$

where $N_0 = 2m^*k_{\mathrm{F}}/\pi^2$ is the density of states at the Fermi surface of nuclear matter, m^* is the effective nucleon mass, and k_{F} is the nucleon Fermi momentum. Taking $m^* = 0.75m_n$ as our fiducial value for the effective mass, we use parameters from [2]

and [6]: $F_0 = -0.28$; $F_0' = 0.95$; $G_0 = 0$; $G_0' = 1.7$, obtaining,

$$v_1 = -7.4 \times 10^{-6} \text{ MeV}^{-2},$$
$$v_2 = 2.5 \times 10^{-5} \text{ MeV}^{-2},$$
$$v_3 = 0,$$
$$v_4 = 4.5 \times 10^{-5} \text{ MeV}^{-2}. \tag{106}$$

For other values of the effective mass, we keep these potentials at the same value, which is to say we assume that the Landau parameters are proportional to m^*/m.

The form for the Gamow–Teller matrix, $S^A(q, \omega)$, is the same as that for S, except that the potential matrix is replaced by v^A

$$v^A = \begin{pmatrix} v_3 + v_4 & v_3 - v_4 \\ v_3 - v_4 & v_3 + v_4 \end{pmatrix}.$$

Taking the matrix inverses leads to the following forms for the combinations of structure functions that appear in Eq. (100)

$$S_{nn}(q, \omega) = 2 \operatorname{Im}\left[\Pi_n^{(0)} D_V^{-1} \right]\left(1 - e^{-\beta\omega}\right)^{-1}, \tag{107}$$

where

$$D_V = 1 - (v_1 + v_2)\Pi_n^{(0)} - (v_1 - v_2)^2 \Pi_n^{(0)} \Pi_p^{(0)} Q_V^{-1}. \tag{108}$$

Q_V is given by the expression:

$$Q_V = 1 - 4\pi e^2 \left(q^2 + q_{\text{TF}}^2\right)^{-1} \Pi_p^{(0)} - (v_1 + v_2)\Pi_p^{(0)}. \tag{109}$$

If, as in Eq. (106), we take $v_3 = 0$, we obtain the simple result for the axial–current terms,

$$S_A(q, \omega) = 2 \operatorname{Im}\left[\frac{\Pi_p^{(0)}(q, \omega) + \Pi_n^{(0)}(q, \omega)}{1 - v_4[\Pi_p^{(0)}(q, \omega) + \Pi_n^{(0)}(q, \omega)]} \right]\left(1 - e^{-\beta\omega}\right)^{-1}. \tag{110}$$

For the Fermi term, since $c_V^{(p)} = 1/2 - 2\sin^2\theta_W \sim 0$, we drop the proton structure function in Eq. (100). Furthermore, we use the potential parameters given in Eq. (106), and in Eq. (108) we drop the third term. This term would have been significant had it not been for the Coulomb term in the denominator, an illustration of the importance of the explicit inclusion of Coulomb forces, even for the neutron density correlations. Since the v_is are all real, we obtain for the structure factors used in Eq. (100),

$$S_{\text{F}}(q, \omega) = 2 \operatorname{Im} \Pi_n^{(0)}\left(1 - e^{-\beta\omega}\right)^{-1} \mathcal{C}_V^{-1}, \tag{111}$$

where

$$\mathcal{C}_V = \left(1 - v_{\text{F}} \operatorname{Re} \Pi_n^{(0)}\right)^2 + v_{\text{F}}^2\left(\operatorname{Im} \Pi_n^{(0)}\right)^2, \tag{112}$$

and

$$S_A(q, \omega) = 2\left[\operatorname{Im} \Pi_p^{(0)}(q, \omega) + \operatorname{Im} \Pi_n^{(0)}(q, \omega)\right]\left(1 - e^{-\beta\omega}\right)^{-1} \mathcal{C}_{\mathcal{A}}^{-1}, \tag{113}$$
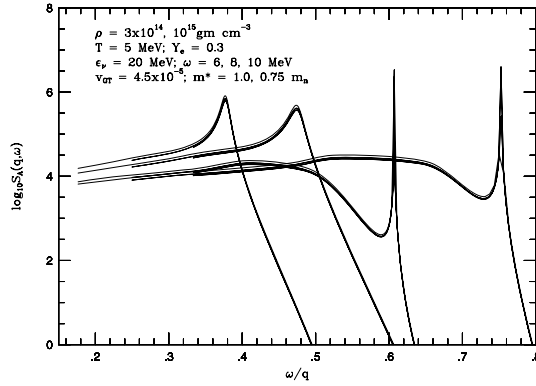
Fig. 8. $\log_{10}$ of the Gamow–Teller structure function versus ω/q for an incident neutrino energy of 20 MeV, energy transfers, ω, of 6, 8, and 10 MeV, two values of the effective mass ($m^* = [0.75m_n, 1.0m_n]$) and two values of the density ($\rho = 3 \times 10^{14}$ and 10^{15} g cm^{-3}). A temperature of 5 MeV and a Y_e of 0.3 were used, as was the default v_{GT} ($= 4.5 \times 10^{-5}$). (Figure taken from Burrows and Sawyer [13].)

where

$$\mathcal{C}_{\mathcal{A}} = \mathcal{C}_{\mathcal{A}1} + \mathcal{C}_{\mathcal{A}2}. \tag{114}$$

$\mathcal{C}_{\mathcal{A}1}$ and $\mathcal{C}_{\mathcal{A}2}$ are given by the expressions:

$$\mathcal{C}_{\mathcal{A}1} = \left[1 - v_{GT} \left(\text{Re}\, \Pi_p^{(0)}(q, \omega) + \text{Re}\, \Pi_n^{(0)}(q, \omega) \right) \right]^2 \tag{115}$$

and

$$\mathcal{C}_{\mathcal{A}2} = v_{GT}^2 \left[\text{Im}\, \Pi_p^{(0)}(q, \omega) + \text{Im}\, \Pi_n^{(0)}(q, \omega) \right]^2. \tag{116}$$

The F in $S_F(q, \omega)$ and the A in $S_A(q, \omega)$ stand for Fermi and Gamow–Teller (axial) and v_F and v_{GT} equal ($v_1 + v_2$) and v_4, respectively, in Fermi Liquid Theory. $S_A(q, \omega)$ in Eq. (113) is now the entire axial term in Eq. (100). $\mathcal{C}_{\mathcal{V},\mathcal{A}}$ is the correction factor due to many-body effects for a given momentum transfer (or scattering angle) and energy transfer. A similar procedure is employed for calculating the many-body corrections to the charged-current rates [14]. Fig. 8 portrays $S_A(q, \omega)$ versus ω/q for representative parameters and clearly indicates the resonances and Čerenkov kinematics.

6.3.2. Multi-pair excitations and the tensor force

The simple model, based on Fermi Liquid Theory and the Random Phase Approximation with central interactions, is rudimentary and relies on the poorly constrained determinations of the Landau parameters. While we can expect this simple analysis to capture qualitative aspects of many-body correlations it is not suitable for quantitative predictions. It has two important shortcomings, namely the neglect of multi-pair excitations and non-central interactions such as the tensor force (pion exchange), which is known to be important in nuclear systems. The discussions in Section 6.1 regarding the response of the ion–plasma clearly emphasized the need to incorporate finite propagation lifetimes for quasi-particles due to collisional damping. The role of collisional damping in the low-energy response is particularly well studied for the case of low-energy photon production

from bremsstrahlung in many-particle systems and is called the Landau–Pomeranchuk–Migdal effect. Similar effects were first investigated in the context of the response of nuclear matter by Raffelt and Seckel [53]. They found that the rate of spin fluctuations $(1/\tau_{\text{spin}})$ due to nucleon–nucleon collisions in the medium is rapid compared to the typical energy transfer ω in neutrino scattering. Consequently, the axial charge is dynamically screened for small $\omega \lesssim \tau_{\text{spin}}^{-1}$, resulting in a suppression of the low-energy axial response.

The redistribution of response strength in energy is a generic feature of many-particle systems arising due to the finite lifetime of quasi-particles. However, the situation in nuclear systems is unique due to the presence of a strong tensor force. This has recently been clarified by Olsson and Pethick [51]. The evolution of nucleon spin is dominated by tensor interactions, especially because the nucleon spin operator $\hat{\sigma}$ does not commute with the tensor operator in the nuclear Hamiltonian. The F-sum rule, discussed earlier in Section 6.1, for the spin response function does not vanish in the long-wavelength limit, since $[\mathcal{H}_{\text{tensor}}, \hat{\sigma}] \neq 0$. Further, the relationship between the spin susceptibility and the Landau parameters is modified due to presence of the tensor interaction (see [51] for these revised relations). The preceding discussion indicates that interactions that do not commute with the spin operator may be especially important in determining the low-energy response. Olsson and Pethick [51] estimate that as much as 60% of the low-energy axial response at long wavelength may reside in multi-particle excitations. This preliminary estimate warrants further investigation requiring both the inclusion of the tensor force and multi-pair excitations in the axial response.

When multi-pair excitations become important it is appropriate to work in terms of a correlated basis states rather than single particle bare neutron and proton states. The correlated basis states are expected to be close to the energy eigenstates of the system. Consequently, in this basis the residual interactions are weak. Further, the ground and excited states in the correlated basis states contain multi-particle hole states and the quasi-particles of the correlated basis are superpositions of neutron and proton states of both spins. This is particularly relevant for nuclear matter, where pion exchange can transform both spin and isospin of the bare nucleons. Recently, Cowell and Pandharipande [18] have computed weak interaction matrix elements in the correlated basis obtained using a two-body cluster expansion. They find that spin and iso-spin correlations play an important role and result in quenching the weak interaction transition rates by 20–25% at low energy.

6.3.3. Relativistic RPA

The RPA polarization tensors that enter the neutrino scattering and absorption rates in a relativistic frame-work have been computed previously by Horowitz and Wehrberger [32] and Reddy et al. [60]. The specific form of the polarization tensor in relativistic random phase approximation (RRPA) follows from the structure of the bubble sum shown in Fig. 7. For a one-component Fermi system, such as neutron matter, the polarization functions appearing in Eq. (51) are replaced by

$$\Pi_{\mu\nu}^{\text{RPA}} = \Pi_{\mu\nu}^{\text{MF}} + \Pi_{\mu\alpha}^{\text{RPA}} D_{\alpha\beta} \Pi_{\beta\nu}^{\text{MF}}, \tag{117}$$

where $D_{\alpha\beta}$, is the relativistic equivalent of the potential matrix defined in Section 6.3.1. It describes the interaction between neutrons and Π_{MF} is the polarization tensor in Eq. (66), but with the Green's functions for neutrons computed in the mean-field approximation. In

relativistic mean-field theories (RMF), which are inspired by the Walecka model, nucleons interact via the exchange of (fictitious) scalar, isoscalar–vector, and isovector–vector mesons (for recent review of RMF models see [63]). The structure of $D_{\alpha\beta}$ and the mean-field Green's functions in RMF theory may be found in [32].

The neutrino mean free paths computed in the context of these models indicate a moderate suppression of 10–20% in the neutrino cross sections at nuclear density. Despite the strong coupling between nucleons, the suppression is modest. This is because the interactions in RMF models primarily affect the vector response, while the neutrino scattering is dominated by the axial response. The RMF model is constrained by its mean field predictions for the empirical properties of *spin saturated* matter. It is necessary to supplement the RMF model with additional spin dependent interactions such as a pion exchange which do not contribute to the ground state properties in the Hartree or mean field approximation. However, these interactions modify the RRPA response. Model calculations in the RRPA which include spin–isospin dependent interactions (pion exchange and phenomenological short-range interactions) have been performed by Reddy et al. [60]. The results of these studies indicate that neutrino mean free path computed in RPA are 2–3 times larger than in the uncorrelated system [60]. This large suppression, which is similar to those encountered in the non-relativistic models, is due to repulsive forces in the spin–isospin channels.

As mentioned earlier, RRPA is the self-consistent response of RMF models with vector and scalar interactions. It ensures thermodynamic consistency, i.e., it satisfies the compressibility sum rules discussed in Section 6.1.2. However, the cross sections are not greatly changed by interactions. In contrast, interactions in the spin–isospin channel do not affect the Hartree or mean-field ground state, but modify the neutrino opacity calculated in RPA. This underscores the need for detailed studies of the spin and spin–isospin response in nuclear models. To date, supernova simulations have employed equations of state (EOS) that are based on the mean-field approximation, including non-relativistic EOS's such as those due to [42]. Spin and spin–isospin susceptibility of these models remain largely unconstrained by either empirical data or input from microscopic calculations of nuclear matter.

7. e^+e^- annihilation

Ignoring phase-space blocking of neutrinos in the final state and taking the relativistic limit ($m_e \to 0$), the total electron–positron annihilation rate into neutrino–anti-neutrino pairs can be written in terms of the electron and positron phase-space densities ($\mathcal{F}$) [19]:

$$Q_{\nu_e\bar\nu_e} = K_i \left(\frac{1}{m_ec^2}\right)^2 \left(\frac{1}{\hbar c}\right)^6 \iint \mathcal{F}_{e^-}\mathcal{F}_{e^+}\left(\varepsilon_{e^-}^4\varepsilon_{e^+}^3 + \varepsilon_{e^-}^3\varepsilon_{e^+}^4\right) d\varepsilon_{e^-}\, d\varepsilon_{e^+}, \qquad (118)$$

where $K_i = (1/18\pi^4)c\sigma_o(C_V'^2 + C_A'^2)$. Again, $C_V' = 1/2 + 2\sin^2\theta_W$ for electron types, $C_V' = -1/2 + 2\sin^2\theta_W$ for ν_μ and ν_τ types, and $C_A'^2 = (1/2)^2$. Rewriting Eq. (118) in terms of the Fermi integral $F_n(\eta)$, we obtain:

$$Q_{\nu_e\bar\nu_e} = K_i(kT)\left(\frac{kT}{m_ec^2}\right)^2\left(\frac{kT}{\hbar c}\right)^6\left[F_4(\eta_e)F_3(-\eta_e) + F_4(-\eta_e)F_3(\eta_e)\right], \qquad (119)$$

where $\eta_e \equiv \mu_e/kT$ and

$$F_n(\eta) \equiv \int\limits_0^\infty \frac{x^n}{e^{x-\eta}+1} dx. \tag{120}$$

Integrating Eq. (118), we obtain

$$Q_{\nu_e \bar{\nu}_e} \simeq 9.7615 \times 10^{24} \left[\frac{kT}{\text{MeV}}\right]^9 f(\eta_e) \text{ erg cm}^{-3}\text{ s}^{-1}, \tag{121}$$

where

$$f(\eta_e) = \frac{F_4(\eta_e)F_3(-\eta_e) + F_4(-\eta_e)F_3(\eta_e)}{2F_4(0)F_3(0)}. \tag{122}$$

For $\nu_\mu \bar{\nu}_\mu$ and $\nu_\tau \bar{\nu}_\tau$ production combined,

$$Q_{\nu_{\mu,\tau}\bar{\nu}_{\mu,\tau}} \simeq 4.1724 \times 10^{24} \left[\frac{kT}{\text{MeV}}\right]^9 f(\eta_e) \text{ erg cm}^{-3}\text{ s}^{-1}. \tag{123}$$

One can easily derive the spectrum of the total radiated neutrino energy (ε_T) by inserting a delta function ($\int \delta(\varepsilon_T - \varepsilon_{e^-} - \varepsilon_{e^+}) d\varepsilon_T$) into Eq. (118). Recall that the total energy of the neutrinos in the final state is equal to the sum of the electron and positron energies in the initial state. Integrating first over ε_{e^+} to annihilate the delta function and then over ε_{e^-} to leave a function of ε_T, one obtains:

$$\frac{dQ}{d\varepsilon_T} = K_i \left(\frac{1}{m_e c^2}\right)^2 \left(\frac{1}{\hbar c}\right)^6 \int\limits_0^{\varepsilon_T} \varepsilon_T(\varepsilon_T - \varepsilon_{e^-})^3 \varepsilon_{e^-}^3 \mathcal{F}_{e^-}[\varepsilon_{e^-}]\mathcal{F}_{e^+}[\varepsilon_T - \varepsilon_{e^-}] d\varepsilon_{e^-}. \tag{124}$$

The numerical evaluation of Eq. (124) is straightforward. The average of ε_T is equal to:

$$\langle \varepsilon_T \rangle = \left(\frac{F_4(\eta_e)}{F_3(\eta_e)} + \frac{F_4(-\eta_e)}{F_3(-\eta_e)}\right) T, \tag{125}$$

which near $\eta_e \sim 0$ is $\sim 8T$ and for $\eta_e \gg 1$ is $\sim 4T(1 + \eta_e/5)$.

However, while the total energy loss rate (Eq. (121)) and the spectrum of ε_T pose no great mathematical problems, the production spectrum of an individual neutrino is not so easily reduced to a simple integral or to an analytic expression. This is due primarily to the awkward integration of the angular phase space terms, while subject to the momentum conservation delta function, and to the explicit dependence of the matrix elements on the electron/neutrino angles. From [19], averaging over initial states and summing over final states, the matrix element for the $e^+ e^- \to \nu\bar{\nu}$ process in the $m_e = 0$ limit is:

$$\frac{1}{4}\sum_s |\mathcal{M}|^2 = 16G^2\big[(C_V' + C_A')^2 \mathbf{p} \cdot \mathbf{q}_{\bar{\nu}}\mathbf{p}' \cdot \mathbf{q}_\nu + (C_V' - C_A')^2 \mathbf{p} \cdot \mathbf{q}_\nu\mathbf{p}' \cdot \mathbf{q}_{\bar{\nu}}\big], \tag{126}$$

where p and p' are the four-momenta of the electron and positron, respectively, and q_ν and $q_{\bar{\nu}}$ are the four-momenta of the neutrino and anti-neutrino, respectively. Using the formalism of [7] and Fermi's Golden rule, expanding the production kernel in the traditional

truncated Legendre series, performing the trivial angular integrals, taking the non-trivial angular integrals from [7], and ignoring final-state neutrino blocking, we obtain for the single-neutrino source spectrum due to e^+e^- annihilation:

$$\frac{dQ}{d\varepsilon_\nu} = \frac{8\pi^2}{(2\pi\hbar c)^6}\varepsilon_\nu^3 \int\limits_0^\infty d\varepsilon_{\bar\nu}\, \varepsilon_{\bar\nu}^2 \Phi_0^p(\varepsilon_\nu, \varepsilon_{\bar\nu}), \tag{127}$$

where

$$\Phi_0^p(\varepsilon_\nu, \varepsilon_{\bar\nu}) = \frac{G^2}{\pi} \int\limits_0^{\varepsilon_\nu+\varepsilon_{\bar\nu}} d\varepsilon_{e^-}\, \mathcal{F}_{e^-}[\varepsilon_{e^-}]\mathcal{F}_{e^+}[\varepsilon_\nu + \varepsilon_{\bar\nu} - \varepsilon_{e^-}]H_0(\varepsilon_\nu, \varepsilon_{\bar\nu}, \varepsilon_{e^-}), \tag{128}$$

and

$$H_0(\varepsilon_\nu, \varepsilon_{\bar\nu}, \varepsilon_{e^-}) = (C_V' + C_A')^2 J_0^I(\varepsilon_\nu, \varepsilon_{\bar\nu}, \varepsilon_{e^-}) + (C_V' - C_A')^2 J_0^{II}(\varepsilon_\nu, \varepsilon_{\bar\nu}, \varepsilon_{e^-}). \tag{129}$$

The J_0s in Eq. (129) come from the more obdurate angular integrals required by the dot products in Eq. (126) and the momentum delta function and have the symmetry:

$$J_0^I(\varepsilon_\nu, \varepsilon_{\bar\nu}, \varepsilon_{e^-}) = J_0^{II}(\varepsilon_{\bar\nu}, \varepsilon_\nu, \varepsilon_{e^-}). \tag{130}$$

From Eqs. (127) and (129), we see that the differences between the spectra of the ν_e and ν_μ neutrinos flow solely from their correspondingly different values of $(C_V' + C_A')^2$ and $(C_V' - C_A')^2$. One can use 4-point Gauss–Legendre integration to calculate Eq. (128) and 16-point Gauss–Laguerre integration to calculate Eq. (127).

At small η_e, the e^+e^- annihilation spectra and total energy loss rates for the ν_e and $\bar\nu_e$ neutrinos are similar, as are the average emitted ν_e and $\bar\nu_e$ neutrino energies. However, as η_e increases, both the total energy radiated in $\bar\nu_e$ neutrinos and the average $\bar\nu_e$ energy start to lag the corresponding quantities for the ν_e neutrinos. This is true despite the fact that the total number of ν_e and $\bar\nu_e$ neutrinos radiated is the same. If final-state blocking is ignored, $\langle\varepsilon_i\rangle/T$ is a function of η_e alone, becoming linear with η_e at high η_e and one half of Eq. (125) (~ 4.0) at low η_e. Note also that $\langle\varepsilon_{\nu_\mu}\rangle/T$ and $\langle\varepsilon_{\bar\nu_\mu}\rangle/T$ are closer to one another than are $\langle\varepsilon_{\nu_e}\rangle/T$ and $\langle\varepsilon_{\bar\nu_e}\rangle/T$. The individual production spectra vary in peak strength, in peak energy, and in low-energy shape, but they are quite similar on the high-energy tail. Due to the parity-violating matrix element for the $e^+e^- \to \nu\bar\nu$ process and the fact that η_e is positive, the anti-neutrino spectra of all species are softer than the neutrino spectra. The pair sums of the integrals under these curves are given by Eqs. (121) and (123). For $\eta_e = 0$, 50% of the pair energy emission of electron types is in $\bar\nu_e$ neutrinos, but at $\eta_e = 10$ only 42% of this total energy is in $\bar\nu_e$ neutrinos. However, at $\eta_e = 10$, the $\bar\nu_\mu$ neutrinos still constitute 48.5% of the $\nu_\mu/\bar\nu_\mu$ pair emission. These differences reflect differences in the corresponding coupling constants C_V' and C_A'.

8. $\nu_i \bar{\nu}_i$ annihilation

In the limit of high temperatures and ignoring electron phase space blocking, the $\nu_i \bar{\nu}_i$ annihilation rate into $e^+ e^-$ pairs can be written [38]:

$$Q_{\nu_i \bar{\nu}_i} = 4 K_i \pi^4 \left(\frac{1}{m_e c^2}\right)\left(\frac{4\pi}{c}\right)^2 \iint \Phi' J_{\nu_i} J_{\bar{\nu}_i}(\epsilon_{\nu_i} + \epsilon_{\bar{\nu}_i}) \, d\epsilon_{\nu_i} \, d\epsilon_{\bar{\nu}_i}, \qquad (131)$$

where J_ν is the zeroth moment of the radiation field, ε_ν is the neutrino energy, K_i is defined as before (i.e., $K_i = (1/18\pi^4) c\sigma_o(C_V'^2 + C_A'^2)$), and

$$\Phi'\big(\langle\mu_{\nu_i}\rangle, \langle\mu_{\bar{\nu}_i}\rangle, p_{\nu_i}, p_{\bar{\nu}_i}\big) = \frac{3}{4}\left[1 - 2\langle\mu_{\nu_i}\rangle\langle\mu_{\bar{\nu}_i}\rangle + p_{\nu_i} p_{\bar{\nu}_i} + \frac{1}{2}(1 - p_{\nu_i})(1 - p_{\bar{\nu}_i})\right], \qquad (132)$$

where the flux factor $\langle\mu_{\nu_i}\rangle = H_\nu/J_\nu$ and the Eddington factor $p_\nu = \langle\mu_{\nu_i}^2\rangle = P_\nu/J_\nu$. Eq. (131) can be rewritten in terms of the invariant distribution functions $\mathcal{F}_\nu$:

$$Q_{\nu_i \bar{\nu}_i} = K_i \left(\frac{1}{m_e c^2}\right)^2 \left(\frac{1}{\hbar c}\right)^6 \iint \Phi' \mathcal{F}_{\nu_i} \mathcal{F}_{\bar{\nu}_i} \big(\varepsilon_{\nu_i}^4 \varepsilon_{\bar{\nu}_i}^3 + \varepsilon_{\nu_i}^3 \varepsilon_{\bar{\nu}_i}^4\big) \, d\varepsilon_{\nu_i} \, d\varepsilon_{\bar{\nu}_i}. \qquad (133)$$

Note that when the radiation field is isotropic ($\Phi' = 1$) and when $\eta_e = 0$ the total rate for $e^+ e^-$ annihilation given in Eq. (118) equals that for $\nu_i \bar{\nu}_i$ annihilation given in Eq. (133), as expected. Buras et al. [9] have addressed the related and interesting process of $\nu_i \bar{\nu}_i \rightarrow \nu_j \bar{\nu}_j$. We refer to that paper for a discussion of the relevance and rates of this process.

9. Nucleon–nucleon bremsstrahlung

A production process for neutrino/anti-neutrino pairs that has recently received attention in the supernova context is neutral-current nucleon–nucleon bremsstrahlung ($n_1 + n_2 \rightarrow n_3 + n_4 + \nu\bar{\nu}$). Its importance in the cooling of old neutron stars, for which the nucleons are quite degenerate, has been recognized for years [20,22], but only in the last few years has it been studied for its potential importance in the quasi-degenerate to non-degenerate atmospheres of protoneutron stars and supernovae [16,28,64,65]. Neutron–neutron, proton–proton, and neutron–proton bremsstrahlung are all important, with the latter the most important for symmetric matter. As a source of ν_e and $\bar{\nu}_e$ neutrinos, nucleon–nucleon bremsstrahlung cannot compete with the charged-current capture processes. However, for a range of temperatures and densities realized in supernova cores, it may compete with $e^+ e^-$ annihilation as a source for ν_μ, $\bar{\nu}_\mu$, ν_τ, and $\bar{\nu}_\tau$ neutrinos ("ν_μ"s). The major obstacles to obtaining accurate estimates of the emissivity of this process are our poor knowledge of the nucleon–nucleon potential, of the degree of suitability of the Born Approximation, and of the magnitude of many-body effects [5,28,54]. Since the nucleons in protoneutron star atmospheres are not degenerate, we present here a calculation of the total and differential emissivities of this process in that limit and assume a one-pion exchange (OPE) potential model to calculate the nuclear matrix element. For the corresponding calculation for arbitrary nucleon degeneracy, the reader is referred to [65]. The formalism we employ has

been heavily influenced by those of [5] and [28], to which the reader is referred for details and further explanations.

Our focus is on obtaining a useful single-neutrino final-state emission (source) spectrum, as well as a final-state pair energy spectrum and the total emission rate. For this, we start with Fermi's Golden Rule for the total rate per neutrino species:

$$Q_{nb} = (2\pi)^4 \int \left[\prod_{i=1}^{4} \frac{d^3\vec{p}_i}{(2\pi)^3} \right] \frac{d^3\vec{q}_\nu}{(2\pi)^3 2\omega_\nu} \frac{d^3\vec{q}_{\bar{\nu}}}{(2\pi)^3 2\omega_{\bar{\nu}}} \omega \sum_s |\mathcal{M}|^2 \delta^4(\mathbf{P}) \, \Xi_{\text{brems}},$$

where

$$\Xi_{\text{brems}} = \mathcal{F}_1 \mathcal{F}_2 (1 - \mathcal{F}_3)(1 - \mathcal{F}_4), \tag{134}$$

$\delta^4(\mathbf{P})$ is four-momentum conservation delta function, ω is the energy of the final-state neutrino pair, $(\omega_\nu, \vec{q}_\nu)$ and $(\omega_{\bar{\nu}}, \vec{q}_{\bar{\nu}})$ are the energy and momentum of the neutrino and antineutrino, respectively, and $\vec{p}_i$ is the momentum of nucleon i. Final-state neutrino and antineutrino blocking have been dropped.

The necessary ingredients for the integration of Eq. (134) are the matrix element for the interaction and a workable procedure for handling the phase-space terms, constrained by the conservation laws. We follow [5] for both of these elements. In particular, we assume for the $n + n \to n + n + \nu\bar{\nu}$ process that the matrix element is:

$$\sum_s |\mathcal{M}|^2 = \frac{64}{4} G_{\text{F}}^2 (f/m_\pi)^4 g_A^2 \left[\left(\frac{k^2}{k^2 + m_\pi^2} \right)^2 + \cdots \right] \frac{\omega_\nu \omega_{\bar{\nu}}}{\omega^2} = A \frac{\omega_\nu \omega_{\bar{\nu}}}{\omega^2}, \tag{135}$$

where the 4 in the denominator accounts for the spin average for identical nucleons, G_{F} is the weak coupling constant, f (~ 1.0) is the pion–nucleon coupling constant, g_A is the axial-vector coupling constant, the term in brackets is from the OPE propagator plus exchange and cross terms, k is the nucleon momentum transfer, and m_π is the pion mass. In Eq. (135), we have dropped $\vec{q}_\nu \cdot \vec{k}$ terms from the weak part of the total matrix element. To further simplify the calculation, we set the "propagator" term equal to a constant ζ, a number of order unity, and absorb into ζ all interaction ambiguities.

Recently, Hanhart, Phillips and Reddy [27] have addressed these momentum terms in the context of axion emission and $\nu_\mu\bar{\nu}_\mu$ production in supernovae. In an effort to make contact with the approximation to the matrix element we present here, they plot ζ as a function of average relative thermal nucleon momentum ($\bar{p}$; Phillips, private communication). The function peaks for $\zeta(\bar{p})$ between 150–200 MeV at $\zeta \simeq 0.47$. At $\bar{p} = 50$ MeV $\zeta \simeq 0.08$ and at $\bar{p} = 500$ MeV $\zeta \simeq 0.27$. We are most interested in the region around the ν_μ neutrinospheres, where the emergent spectrum might be most affected by nucleon–nucleon bremsstrahlung. Mass densities and temperatures in this region might be 10^{12}–10^{13} g cm^{-3} and 5–10 MeV, respectively. We estimate $\bar{p}$ in this regime to be ~ 175 MeV and take $\zeta = 0.5$ for all thermodynamical points. The constant A in Eq. (135) remains.

Inserting a $\int \delta(\omega - \omega_\nu - \omega_{\bar{\nu}}) \, d\omega$ by the neutrino phase space terms times $\omega \omega_\nu \omega_{\bar{\nu}}/\omega^2$ and integrating over $\omega_{\bar{\nu}}$ yields:

$$\int \omega \frac{\omega_\nu \omega_{\bar{\nu}}}{\omega^2} \frac{d^3\vec{q}_\nu}{(2\pi)^3 2\omega_\nu} \frac{d^3\vec{q}_{\bar{\nu}}}{(2\pi)^3 2\omega_{\bar{\nu}}} \to \frac{1}{(2\pi)^4} \int_0^\infty \int_0^\omega \frac{\omega_\nu^2 (\omega - \omega_\nu)^2}{\omega} \, d\omega_\nu \, d\omega, \tag{136}$$

where again ω equals $(\omega_\nu + \omega_{\bar\nu})$. If we integrate over ω_ν, we can derive the ω spectrum. A further integration over ω will result in the total volumetric energy emission rate. If we delay such an integration, after the nucleon phase space sector has been reduced to a function of ω and if we multiply Eq. (134) and/or Eq. (136) by ω_ν/ω, an integration over ω from ω_ν to infinity will leave the emission spectrum for the single final-state neutrino. This is of central use in multi-energy group transport calculations and with this differential emissivity and Kirchhoff's Law (Section 2) we can derive an absorptive opacity.

Whatever our final goal, we need to reduce the nucleon phase space integrals and to do this we use the coordinates and approach of [5]. We define new momenta: $p_+ = (p_1 + p_2)/2$, $p_- = (p_1 - p_2)/2$, $p_{3c} = p_3 - p_+$, and $p_{4c} = p_4 - p_+$, where nucleons 1 and 2 are in the initial state. Useful direction cosines are $\gamma_1 = p_+ \cdot p_-/|p_+||p_-|$ and $\gamma_c = p_+ \cdot p_{3c}/|p_+||p_{3c}|$. Defining $u_i = p_i^2/2mT$ and using energy and momentum conservation, we can show that:

$$d^3p_1\,d^3p_2 = 8d^3p_+\,d^3p_-,$$
$$\omega = 2T(u_- - u_{3c}),$$
$$u_{1,2} = u_+ + u_- \pm 2(u_+u_-)^{1/2}\gamma_1,$$
$$u_{3,4} = u_+ + u_{3c} \pm 2(u_+u_{3c})^{1/2}\gamma_c. \tag{137}$$

In the non-degenerate limit, the $\mathcal{F}_1\mathcal{F}_2(1 - \mathcal{F}_3)(1 - \mathcal{F}_4)$ term reduces to $e^{2y}e^{-2(u_+ + u_-)}$, where y is the nucleon degeneracy factor. Using Eq. (137), we see that the quantity $(u_+ + u_-)$ is independent of both γ_1 and γ_c. This is a great simplification and makes the angle integrations trivial. Annihilating d^3p_4 with the momentum delta function in Eq. (134), noting that $p_i^2\,dp = \frac{(2mT)^{3/2}}{2}u_i^{1/2}\,du_i$, pairing the remaining energy delta function with u_-, and integrating u_+ from 0 to ∞, we obtain:

$$dQ_{nb} = \frac{Am^{4.5}}{2^8 \times 3 \times 5\pi^{8.5}}T^{7.5}e^{2y}e^{-\omega/T}(\omega/T)^4\left[\int_0^\infty e^{-x}\left(x^2 + x\omega/T\right)^{1/2}dx\right]d\omega. \tag{138}$$

The variable x over which we are integrating in Eq. (138) is equal to $2u_{3c}$. That integral is analytic and yields:

$$\int_0^\infty e^{-x}\left(x^2 + x\omega/T\right)^{1/2}dx = \eta e^\eta K_1(\eta), \tag{139}$$

where K_1 is the standard modified Bessel function of imaginary argument, related to the Hankel functions, and $\eta = \omega/2T$. Hence, the ω spectrum is given by:

$$\frac{dQ_{nb}}{d\omega} \propto e^{-\omega/2T}\omega^5 K_1(\omega/2T). \tag{140}$$

It can easily be shown that $\langle\omega\rangle = 4.364T$. Integrating Eq. (138) over ω and using the thermodynamic identity in the non-degenerate limit:

$$e^y = \left(\frac{2\pi}{mT}\right)^{3/2}n_n/2, \tag{141}$$

where n_n is the density of neutrons (in this case), we derive for the total neutron–neutron bremsstrahlung emissivity of a single neutrino pair:

$$Q_{nb} = 1.04 \times 10^{30} \zeta (X_n \rho_{14})^2 \left(\frac{T}{\mathrm{MeV}} \right)^{5.5} \mathrm{erg\,cm^{-3}\,s^{-1}}, \tag{142}$$

where ρ_{14} is the mass density in units of 10^{14} gm cm^{-3} and X_n is the neutron mass fraction. Interestingly, this is within 30% of the result in [64], even though he has substituted, without much justification, $(1 + \omega/2T)$ for the integral in Eq. (138) ($[1 + (\pi\eta/2)^{1/2}]$ is a better approximation). The proton–proton and neutron–proton processes can be handled similarly and the total bremsstrahlung rate is then obtained by substituting $X_n^2 + X_p^2 + \frac{28}{3} X_n X_p$ for X_n^2 in Eq. (142) [5]. At $X_n = 0.7$, $X_p = 0.3$, $\rho = 10^{12}$ gm cm^{-3}, and $T = 10$ MeV, and taking the ratio of augmented Eq. (142) to Eq. (123), we obtain the promising ratio of $\sim 5\zeta$. Setting the correction factor ζ equal to ~ 0.5 [27], we find that near and just deeper than the ν_μ neutrinosphere, bremsstrahlung is larger than classical pair production.

If in Eq. (136) we do not integrate over ω_ν, but at the end of the calculation we integrate over ω from ω_ν to ∞, after some manipulation we obtain the single neutrino emissivity spectrum:

$$\frac{dQ'_{nb}}{d\omega_\nu} = 2C \left(\frac{Q_{nb}}{T^4} \right) \omega_\nu^3 \int_{\eta_\nu}^{\infty} \frac{e^{-\eta}}{\eta} K_1(\eta)(\eta - \eta_\nu)^2 \, d\eta \tag{143}$$

$$= 2C \left(\frac{Q_{nb}}{T^4} \right) \omega_\nu^3 \int_{1}^{\infty} \frac{e^{-2\eta_\nu \xi}}{\xi^3} \left(\xi^2 - \xi \right)^{1/2} d\xi, \tag{144}$$

where $\eta_\nu = \omega_\nu/2T$, C is the normalization constant equal to $(3 \times 5 \times 7 \times 11)/2^{11}$ ($\cong 0.564$), and for the second expression we have used the integral representation of $K_1(\eta)$ and reversed the order of integration. In Eq. (144), Q_{nb} is the emissivity for the pair.

Eq. (144) is the approximate neutrino emission spectrum due to nucleon–nucleon bremsstrahlung. A useful fit to Eq. (144), good to better than 3% over the full range of important values of η_ν, is:

$$\frac{dQ'_{nb}}{d\omega_\nu} \cong \frac{0.234 Q_{nb}}{T} \left(\frac{\omega_\nu}{T} \right)^{2.4} e^{-1.1\omega_\nu/T}. \tag{145}$$

Ref. [65] should be consulted for a detailed discussion of nucleon–nucleon bremsstrahlung for arbitrary nucleon degeneracy.

10. Conclusion

The processes that have been described in this paper are essential elements of the neutrino-driven supernova explosion mechanism. Coupling these with radiation-hydrodynamics codes, an equation of state, beta-decay and electron capture microphysics, and nuclear rates, one explores the viability of various scenarios for the explosion of the

cores of massive stars [44,45,56,57]. Recently, [66] have incorporated this neutrino microphysics into simulations of 1D (spherical) core collapse and have investigated the effects on the dynamics, luminosities, and emergent spectra of weak magnetism/recoil, nucleon–nucleon bremsstrahlung, inelastic neutrino–electron scattering, and a host of the cross section corrections described above. The character of the spectra reflect the opacities and sources. In particular, the energy hardness hierarchy from ν_e (softer) to ν_μ (harder) neutrinos is clearly manifest, as is the distinction between the ν_e pre-breakout and post-breakout spectra.

To date, none of the detailed 1D simulations that have been performed explodes and it may be that multi-dimensional effects play a pivotal role in the explosion mechanism [12, 23,24,30,39]. Be that as it may, an understanding of neutrino–matter interactions remains central to unraveling one of the key mysteries of the nuclear universe in which we live.

Acknowledgements

References

[1] M. Aufderheide, I. Fushiki, G. Fuller, T. Weaver, Astrophys. J. 424 (1994) 257.
[2] S.-O. Backman, G.E. Brown, J.A. Niskanen, Phys. Rep. 124 (1985) 1.
[3] G. Baym, C.J. Pethick, Landau Fermi Liquid Theory, Wiley, New York, 1991.
[4] D. Bohm, D. Pines, Phys. Rev. 92 (1953) 609.
[5] R.P. Brinkmann, M.S. Turner, Phys. Rev. D 38 (8) (1988) 2338.
[6] G.E. Brown, M. Rho, Nucl. Phys. A 372 (1981) 397.
[7] S.W. Bruenn, Astrophys. J. Suppl. 58 (1985) 771.
[8] S.W. Bruenn, A. Mezzacappa, Phys. Rev. D 56 (1997) 7529.
[9] R. Buras, H.-Th. Janka, M.Th. Keil, G.G. Raffelt, M. Rampp, Astrophys. J. 587 (2003) 320.
[10] R. Buras, M. Rampp, H.-Th. Janka, K. Kifonidis, Phys. Rev. Lett. 90 (2003) 1101.
[11] A. Burrows, T.J. Mazurek, J.M. Lattimer, Astrophys. J. 251 (1981) 325.
[12] A. Burrows, J. Hayes, B.A. Fryxell, Astrophys. J. 450 (1995) 830.
[13] A. Burrows, R.F. Sawyer, Phys. Rev. C 58 (1998) 554.
[14] A. Burrows, R.F. Sawyer, Phys. Rev. C 59 (1999) 510.
[15] A. Burrows, Nature 403 (2000) 727.
[16] A. Burrows, T. Young, P.A. Pinto, R. Eastman, T. Thompson, Astrophys. J. 539 (2000) 865.
[17] A. Burrows, Prog. Part. Nucl. Phys. 46 (2001) 59.
[18] S. Cowell, V. Pandharipande, Phys. Rev. C 67 (2002) 035504.
[19] D.A. Dicus, Phys. Rev. D 6 (1972) 941.
[20] E. Flowers, P. Sutherland, J.R. Bond, Phys. Rev. D 12 (1975) 316.

[21] D.Z. Freedman, Phys. Rev. D 9 (1974) 1389.
[22] B.L. Friman, O.V. Maxwell, Astrophys. J. 232 (1979) 541.
[23] C.L. Fryer, W. Benz, M. Herant, S. Colgate, Astrophys. J. 516 (1999) 892.
[24] C.L. Fryer, M. Warren, Astrophys. J. 574 (2002) L65.
[25] G. Fuller, Astrophys. J. 252 (1982) 741.
[26] G.M. Fuller, W.A. Fowler, M.J. Newman, Astrophys. J. 252 (1982) 715.
[27] C. Hanhart, D. Phillips, S. Reddy, Phys. Lett. B 499 (2001) 9.
[28] S. Hannestad, G. Raffelt, Astrophys. J. 507 (1998) 339.
[29] J.-P. Hansen, I.R. McDonald, E.L. Pollock, Phys. Rev. D 11 (1975) 1025.
[30] M. Herant, W. Benz, W.R. Hix, C.L. Fryer, S.A. Colgate, Astrophys. J. 435 (1994) 339.
[31] C.J. Horowitz, K. Wehrberger, Nucl. Phys. A 531 (1991) 665.
[32] C.J. Horowitz, K. Wehrberger, Phys. Lett. B 226 (1992) 236.
[33] C.J. Horowitz, Phys. Rev. D 55 (1997) 4577.
[34] C.J. Horowitz, Phys. Rev. D 65 (2002) 043001.
[35] C.J. Horowitz, M.A. Pérez-García, Phys. Rev. C 68 (2003) 025803.
[36] C.J. Horowitz, M.A. Pérez-García, P. Piekarewicz, astro-ph/0401079.
[37] N. Iwamoto, C.J. Pethick, Phys. Rev. D 25 (1982) 313.
[38] H.-T. Janka, Astron. Astrophys. 244 (1991) 378.
[39] H.-Th. Janka, E. Müller, Astron. Astrophys. 306 (1996) 167.
[40] L.P. Kadanoff, P.C. Martin, Ann. Phys. (N.Y.) 24 (1963) 419.
[41] K. Langanke, G. Martinez-Pinedo, Rev. Mod. Phys. 75 (2003) 819.
[42] J.M. Lattimer, F.D. Swesty, Nucl. Phys. A 535 (1991) 331–376.
[43] L.B. Leinson, V.N. Oraevsky, V.B. Semikoz, Phys. Lett. B 209 (1988) 1.
[44] M. Liebendörfer, A. Mezzacappa, F.-K. Thielemann, O.E.B. Messer, W.R. Hix, S.W. Bruenn, Phys. Rev. D 63 (2001) 103004.
[45] M. Liebendörfer, A. Mezzacappa, F.-K. Thielemann, Phys. Rev. D 63 (2001) 104003.
[46] J. Lindhard, Kgl. Danske Videnskab Selskab, Mat. Fys. Medd. 28 (1954) 8.
[47] T. Luu, A. Hungerford, J. Carlson, C. Fryer, S. Reddy, 2004, in preparation.
[48] A. Mezzacappa, S.W. Bruenn, Astrophys. J. 410 (1993) 637.
[49] A. Mezzacappa, S.W. Bruenn, Astrophys. J. 410 (1993) 669.
[50] A. Mezzacappa, S.W. Bruenn, Astrophys. J. 410 (1993) 740.
[51] E. Olsson, C.J. Pethick, Phys. Rev. C 66 (2002) 065803.
[52] J. Pruet, G.M. Fuller, Astrophys. J. Suppl. 149 (2003) 189.
[53] G. Raffelt, D. Seckel, Phys. Rev. D 52 (1995) 1780.
[54] G. Raffelt, D. Seckel, Phys. Rev. Lett. 69 (1998) 2605.
[55] G. Raffelt, Astrophys. J. 561 (2001) 890.
[56] M. Rampp, H.-Th. Janka, Astrophys. J. 539 (2000) L33.
[57] M. Rampp, H.-Th. Janka, Astron. Astrophys. 396 (2002) 331.
[58] D.G. Ravenhall, C.J. Pethick, J.R. Wilson, Phys. Rev. Lett. 50 (1983) 2066.
[59] S. Reddy, M. Prakash, J.M. Lattimer, Phys. Rev. D 58 (1998) 013009.
[60] S. Reddy, M. Prakash, J.M. Lattimer, J.A. Pons, Phys. Rev. C 59 (1999) 2888.
[61] R.F. Sawyer, Phys. Rev. D 11 (1975) 2740.
[62] P.J. Schinder, Astrophys. J. Suppl. 74 (1990) 249.
[63] B.D. Serot, J.D. Walecka, Int. J. Mod. Phys. E 6 (1997) 515.
[64] H. Suzuki, in: Y. Suzuki, K. Nakamura (Eds.), Frontiers of Neutrino Astrophysics, Universal Academy Press, Tokyo, 1993, p. 219.
[65] T.A. Thompson, A. Burrows, J.E. Horvath, Phys. Rev. C 62 (2000) 035802.
[66] T.A. Thompson, A. Burrows, P.A. Pinto, Astrophys. J. 592 (2003) 434.
[67] D.L. Tubbs, D.N. Schramm, Astrophys. J. 201 (1975) 467.
[68] P. Vogel, Phys. Rev. D 29 (1984) 1918.
[69] G. Watanabe, K. Sato, K. Yasuoka, T. Ebisuzaki, Phys. Rev. C 68 (2003) 035806.